AN ABSTRACT OF THE THESIS OF

Alexander P. Albus for the degree of Master of Science in Physics presented on April 6, 1999.

Title: Immersion Energies of Atoms in Jellium.

Redacted for Privacy

Abstract approved: _____   _____

Henri J. F. Jansen

Immersion energies of atoms in a jellium environment were calculated using density functional theory and the Kohn-Sham (KS) equations. It was found that the KS scheme does not destroy an existing axial symmetry of the electron structure of the impurity atom. The definition of phase shifts was extended to those problems and it was shown that they are m-dependent. A suitable cut-off for the l-values was found in the partial wave analysis of the scattered states.

The Kohn-Sham equations were solved numerically on a computer. Results for H and Fe were analyzed. The results for H are in reasonable agreement with previously reported data. Differences are possibly due to a difference in the choice for the cut-off of the l-values.

Immersion Energies of Atoms in Jellium

by

Alexander P. Albus

A Thesis

submitted to

Oregon State University

in partial fulfillment of
the requirements for the
degree of

Master of Science

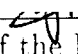Completed April 6, 1999
Commencement June 1999

Master of Science thesis of Alexander P. Albus presented on April 6, 1999

APPROVED:

Redacted for Privacy

Major Professor, representing Physics
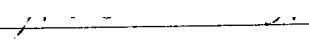
Redacted for Privacy

Chair of the Department of Physics

Redacted for Privacy

Dean of the Graduate School

I understand that my thesis will become part of the permanent collection of Oregon State University libraries. My signature below authorizes release of my thesis to any reader upon request.

Redacted for Privacy

Alexander P. Albus, Author

ACKNOWLEDGMENT

my other friends in Germany, who kept in touch with me during the one and a half years I stayed in the US.

Last but not least, I thank my parents for all their support.

TABLE OF CONTENTS

TABLE OF CONTENTS (Continued)

LIST OF FIGURES

IMMERSION ENERGIES OF ATOMS IN JELLIUM

1. INTRODUCTION

A large variety of properties of condensed matter can be understood by investigating the electronic structure of materials. All electrical, magnetic, optical, and chemical phenomena are examples of this. The richness of these phenomena reflects the complexity of the equations that govern multi-particle electron systems. On the other hand this complexity makes it impossible to solve the equations exactly. A number of approximative methods have been suggested and the most commonly used are perturbation theory, Hartree-Fock theory, and density functional theory. Past experience shows that density functional theory is the most suitable of these to describe the electronic structure of atoms, molecules, and solids.

In this thesis density functional theory is used to calculate the electronic properties of atoms immersed in a jellium environment. In the jellium model there is a uniform positive background charge density and an electron cloud with equal magnitude of charge but opposite sign. The advantage of this model is that the background does not destroy any symmetry of the original system and no additional complexity is added to the equations. Of course, this model is only applicable to systems where the dependence on structure is not critical. The model, however, has been used to successfully study chemisorption on metal surfaces, impurities and

vacancies in metals, optical properties of metals, inter-ionic forces in metals, and binding energies of atoms to large molecules.

The context in which our group is interested in this subject is the magnetic transition of iron atoms when forming a solid. The electronic structure of a free iron atom satisfies Hund's second rule, whereas a single iron atom in a metal does not. It is useful to understand the origin of the violation of Hund's second rule in a solid in order to understand magnetic anisotropy in iron.

Hence we approach the problem by focusing on a single iron atom and approximate all other iron atoms by a uniform background. Starting with a zero background density, which is equivalent to a free iron atom, we increase the background density until the actual density of the conduction electrons in a metal is reached. By calculating the electron distribution for a variety of intermediate densities we hope to understand the origin of the decrease in orbital angular momentum as seen in the violation of Hund's second rule.

The theoretical background is given in chapter 2 for the general, spin-dependent, non-spherical case. Chapter 3 describes the computer programs implemented for this thesis for the spin independent, spherical case only. The extension to spin dependent and non-spherical systems is in progress. The code was implemented in FORTRAN using parts of Sean Fox's and Bob Erickson's previous work. Chapter 4 is a guideline of how to use the program and summarizes the data produced with the program. A complete set of data was obtained for H. In the case of Fe additional work is required.

2. THE THEORETICAL METHODS

2.1. Density Functional Theory

With density functional theory one can find the ground state energy of an interacting many-body system in an external potential. With the Kohn-Sham (KS) equations the problem is reduced to calculating single-particle states. In this section a rough outline of the foundations of density functional theory is given.

As appropriate for many-body problems the second quantized notation is used. In this notation the Hamiltonian of a system of Coulomb-interacting identical particles in a spin dependent external potential is

$$\widehat{H} = \sum_s \int \Psi_s^\dagger(\vec{r})[-\frac{\hbar^2}{2m_0}\vec{\nabla}^2 + V^s(\vec{r})]\Psi_s(\vec{r})d^3\vec{r} +$$
$$\frac{1}{2}\sum_{s,s'} \int \int \Psi_s^\dagger(\vec{r})\Psi_{s'}^\dagger(\vec{r}')\frac{q^2}{|\vec{r}-\vec{r}'|}\Psi_{s'}(\vec{r}')\Psi_s(\vec{r})d^3\vec{r}d^3\vec{r}', \qquad (2.1)$$

where $\Psi_s(\vec{r}), \Psi_s^\dagger(\vec{r})$ are the field operators (s is the spin index and m_0 is the mass of the particles). The specific choice of this Hamiltonian is justified in Appendix A. Let Φ be a state in Fock-space. Then the energy expectation value of this state is

$$E = <\Phi|\widehat{H}|\Phi>$$

and the spin-density of the particles is given by

$$n^s(\vec{r}) = <\Phi|\Psi_s^\dagger(\vec{r})\Psi_s(\vec{r})|\Phi>.$$

The Hohenberg-Kohn theorem (see [1, p.83] and [2, sec. 2.1]) [1] states that the ground state energy is a functional of the densities only. $E = E[n^s]$ (the latter notation is a short for $E[n^{-\frac{2S+1}{2}}, \ldots, n^{+\frac{2S+1}{2}}]$, in particular $E[n^{-\frac{1}{2}}, n^{+\frac{1}{2}}]$ for electrons). The

___

[1] see Appendix B

idea behind the proof of this theorem is to use the fact that the state(s) correspond-
ing to the ground state density has/have to be the eigenstate(s) corresponding to
the lowest energy eigenvalue and that all other energy expectation values are larger
(Ritz-Raleigh principle). One can show by reductio ad absurdum that the external
potential $V^s(\vec{r})$ is uniquely (up to an additive constant) determined once the ground
state density is known or, in other words, that the external potential is a functional
of the ground state density. Hence one can write $E = F_{HK} + \sum_s \int V^s(\vec{r})n^s(\vec{r})d^3\vec{r}$,
where the second term is a functional of the density. The fist term is the expec-
tation value of the kinetic energy plus the interaction energy expectation value. It
turns out to be a unique functional of the density as well. This is easy to see for
a non-degenerate ground state, since the non-degenerate ground state is already a
functional of the density and therefore any expectation value is too. But in [2, p.
9f] it is shown that the same is true for a degenerate ground state.

The Hohenberg-Kohn theorem leads to a great simplification of the problem,
because now one does not have to find the ground state energy by looking for
the ground state in Fock-space but one finds this energy by searching real valued
functions $n^s(\vec{r})$ to minimize the energy-functional.
The theorem, however, does not state what the form of the energy-functional is. Of
course, the classical Coulomb-energy

$$\frac{1}{2}q^2 \int \int \frac{n(\vec{r})n(\vec{r}')}{|\vec{r} - \vec{r}'|}d^3\vec{r}d^3\vec{r}' + q\sum_s \int V^s(\vec{r})n^s(\vec{r})d^3\vec{r}$$

is a part of this energy-functional. With $n(\vec{r}) := \sum_s n^s(\vec{r})$ one can easily see that
the latter expression is a functional of the densities, i.e. is of the desired form. Thus
one writes the energy functional

$$E[n^s] = G[n^s] + \frac{1}{2}q^2 \int \int \frac{n(\vec{r})n(\vec{r}')}{|\vec{r} - \vec{r}'|}d^3\vec{r}d^3\vec{r}' + q\sum_{s'} \int V^{s'}(\vec{r})n^{s'}(\vec{r})d^3\vec{r}.$$

where $G[n^s]$ stands for all contributions to the energy functional, that are not included in the classical Coulomb energy. Of course, $G[n^s]$ still includes the kinetic energy of the particles. But the kinetic energy is mainly a single-particle contribution to the energy functional. If one follows the procedure to reduce the problem to find single-particle states, which is done by virtue of the KS equations (see below), one expects that most of the kinetic energy is already included in the single-particle equations. So one does not have to know the kinetic-energy functional. Until later this functional is referred to as $T[n^s]$ and left unspecified. Everything that is not included in $E[n^s]$ so far contains all many-particle contributions besides the classical Coulomb-energy and is called exchange-correlation energy $E_{xc}[n^s]$. Several approximations are known for $E_{xc}[n^s]$ and in a later section we give one explicit approximation for $E_{xc}[n^s]$.

To summarize, one has $G[n^s] = T[n^s] + E_{xc}[n^s]$ and the energy functional is:

$$E[n^s] = T[n^s] + \frac{1}{2}q^2 \int \int \frac{n(\vec{r})n(\vec{r}')}{|\vec{r} - \vec{r}'|} d^3\vec{r} d^3\vec{r}' +$$
$$E_{xc}[n^s] + q \sum_{s'} \int V^{s'}(\vec{r})n^{s'}(\vec{r})d^3\vec{r}, \qquad (2.2)$$

To find the ground state energy for a fixed number of particles one has to minimize $E[n^s]$ with respect to the n^s under the constraint of spin and charge conservation, $\int n^s(\vec{r})d^3\vec{r} = $ const., i.e. to solve the variational problem $\frac{\delta E[n^{s'}]}{\delta n^s}(\vec{r}) = \mu^s$, where the (constant) Lagrange-multiplier μ^s turns out to be the spin dependent chemical potential of the system (see e.g. [1, section 2.2] and [2, section 2.4]. See also [2, chapter 2] for the proof that one can extend the definition of all functionals, so that the functional derivative is well-defined and the minimum is really the ground state energy).

The reason why this minimization of 2.2 cannot be done directly is —as already mentioned — that the kinetic-energy functional is not known explicitly (except for

the nearly uniform electron gas in Thomas-Fermi theory, where the kinetic energy turns out to be an integral over the density to the power $\frac{5}{3}$).

So the final step to reduce the problem to single-particle equations is to assume $\mathcal{V}_{eff}^s$-representability of the densities $n^s(\vec{r})$. This means, that one can find trial single-particle potentials $\mathcal{V}_{eff}^s(\vec{r})$ so that the solutions of the Schroedinger equation

$$[-\frac{\hbar^2}{2m_0}\vec{\nabla}^2 + q\mathcal{V}_{eff}^s(\vec{r})]\psi_i^s(\vec{r}) = E_i^s\psi_i^s(\vec{r}) \tag{2.3}$$

give

$$n^s(\vec{r}) = \sum_i |\psi_i^s(\vec{r})|^2, \tag{2.4}$$

where the $\psi_i^s(\vec{r})$ are single-particle states and the sum in (2.4) is taken over the lowest occupied states (degeneracies, esp. spin-degeneracies, have to be taken into account here). Physical intuition predicts that well-behaved densities are $\mathcal{V}_{eff}^s$-representable, because one can think of selecting a particle in the system and calculating the potential it 'feels' due to all other particles in the system. The states of this particle are then solutions to (2.3). It turns out, however, that the mathematical proof of this is much more complicated and that the assertion is not even true for a large set of densities (see [2, section 2.3]). For the remainder of this thesis it is assumed that the densities are $\mathcal{V}_{eff}^s$-representable, at least in an approximate sense. Next we have to determine $\mathcal{V}_{eff}^s(\vec{r})$. In our problem

$$\mathcal{V}_{eff}^s(\vec{r}) = V^s(\vec{r}) + q\int\frac{n(\vec{r'})}{|\vec{r}-\vec{r'}|}d^3\vec{r'} + \frac{1}{q}\frac{\delta E_{xc}[n^{s'}]}{\delta n^s}(\vec{r}) + \text{const.}, \tag{2.5}$$

where const. was introduced to ensure that $\mathcal{V}_{eff}^s$ goes to zero for $r \to \infty$. To prove the theorem some formulas of the calculus of variations are required. Here is a list of some that are used later.

A functional derivative is defined by:

$$\int\frac{\delta F[n]}{\delta n}(\vec{r})\delta n(\vec{r})d^3\vec{r} := \frac{d}{d\epsilon}F[n + \epsilon\delta n]|_{\epsilon=0}$$

for any variation $\delta n(\vec{r})$. This definition can be readily extended to space-dependent functionals:

$$\int \frac{\delta G(\vec{r}')[n]}{\delta n}(\vec{r})\delta n(\vec{r})d^3\vec{r} := \frac{d}{d\epsilon}G(\vec{r}')[n+\epsilon\delta n]|_{\epsilon=0}$$

From these definitions the following properties can be easily derived:

1. The functional derivative is linear.

2. $\frac{\delta G^*(\vec{r}')[n]}{\delta n}(\vec{r}) = \left\{\frac{\delta G(\vec{r}')[n]}{\delta n}(\vec{r})\right\}^*$

3. $\frac{\delta \vec{\nabla}'^2 G(\vec{r}')[n]}{\delta n}(\vec{r}) = \vec{\nabla}'^2\left\{\frac{\delta G(\vec{r}')[n]}{\delta n}(\vec{r})\right\}$,

   where $\vec{\nabla}'^2$ is the laplacian with respect to the primed variable.

4. $\frac{\delta \int G(\vec{r}')[n]d^3\vec{r}'}{\delta n}(\vec{r}) = \int \frac{\delta G(\vec{r}')[n]}{\delta n}(\vec{r})d^3\vec{r}'$

5. $\frac{\delta G(\vec{r}')[n]H(\vec{r}')[n]}{\delta n}(\vec{r}) = \frac{\delta G(\vec{r}')[n]}{\delta n}(\vec{r})H(\vec{r}')[n] + G(\vec{r}')[n]\frac{\delta H(\vec{r}')[n]}{\delta n}(\vec{r})$

6. $\frac{\delta \int n(\vec{r}'')f(\vec{r}'',\vec{r}')d^3\vec{r}''}{\delta n}(\vec{r}'') = f(\vec{r},\vec{r}')$

7. From 6. follows:
   $$\frac{\delta n(\vec{r}')}{\delta n}(\vec{r}) = \frac{\delta \int n(\vec{r}'')\delta(\vec{r}'-\vec{r}'')d^3\vec{r}''}{\delta n}(\vec{r}) = \delta(\vec{r}-\vec{r}')$$

8. And from 2. and 5. follows:
   $$\frac{\delta |G(\vec{r}')[n]|^2}{\delta n}(\vec{r}) = \frac{\delta G(\vec{r}')[n]}{\delta n}(\vec{r})(G(\vec{r}')[n])^* + G(\vec{r}')[n](\frac{\delta G(\vec{r}')[n]}{\delta n}(\vec{r}))^*$$

9. $\frac{\delta \int f(n(\vec{r}'))d^3\vec{r}'}{\delta n}(\vec{r}) = \frac{df}{dn}(n(\vec{r}))$

Now we continue with the proof of the theorem 2.5. which is a simplified version of [2, sec. 4.1].

For details see *loc. cit.* From the Hohenberg-Kohn theorem it follows that $V_{eff}(\vec{r})$ is a functional of the ground state density, as are the $\iota_i^s(\vec{r})$ as solutions of (2.3). So one can write (2.2):

$$E[n^{s'}] = \sum_{i,s''} \int (\psi_i^{s''}(\vec{r}')[n^{s'}])^* (-\frac{\hbar^2}{2m_0}\vec{\nabla}'^2)\psi_i^{s''}(\vec{r}')[n^{s'}]d^3\vec{r}' +$$

$$\frac{1}{2}q^2 \int \int \frac{n(\vec{r})n(\vec{r}')}{|\vec{r}-\vec{r}'|}d^3\vec{r}d^3\vec{r}' +$$

$$E_{xc}[n^{s'}] + q\sum_{s''} \int V^{s''}(\vec{r})n^{s''}(\vec{r})d^3\vec{r}, \qquad (2.6)$$

where the kinetic energy is now written in terms of single-particle states.

Applying the functional derivative with respect to the density at the ground state to this equation gives:

$$\mu^s = \frac{\delta E[n^{s'}]}{\delta n^s}(\vec{r}) =$$

$$\sum_{i,s''} \int \{ (\frac{\delta\psi_i^{s''}(\vec{r}')[n^{s'}]}{\delta n^s}(\vec{r}))^* (-\frac{\hbar^2}{2m_0}\vec{\nabla}'^2)\psi_i^{s''}(\vec{r}')[n^{s'}] +$$

$$\frac{\delta\psi_i^{s''}(\vec{r}')[n^{s'}]}{\delta n^s}(\vec{r})(-\frac{\hbar^2}{2m_0}\vec{\nabla}'^2)(\psi_i^{s''}(\vec{r}')[n^{s'}])^* \}d^3\vec{r}'$$

$$+q\sum_{s''}\delta_{s,s''}V^s(\vec{r}) + q^2 \int \frac{n(\vec{r}')}{|\vec{r}-\vec{r}'|}d^3\vec{r}' + \frac{\delta E_{xc}[n^{s'}]}{\delta n^s}(\vec{r}), \qquad (2.7)$$

after using 1., 5., 6., 7., 3., Green's formula to change the Laplacian in the kinetic energy term and the fact that all n^s are varied independently of one another (this gives the $\delta_{s,s''} - term$). Also the chemical potential μ^s was introduced to ensure charge conservation (see above). With (2.3) one can simplify the first integral in (2.7) to

$$\sum_{i,s''} \int \{ (\frac{\delta\psi_i^{s''}(\vec{r}')[n^{s'}]}{\delta n^s}(\vec{r}))^* (E_i^{s''} - V_{eff}^{s''}(\vec{r}'))\psi_i^{s''}(\vec{r}')[n^{s'}] +$$

$$\frac{\delta\psi_i^{s''}(\vec{r}')[n^{s'}]}{\delta n^s}(\vec{r})(E_i^{s''} - V_{eff}^{s''}(\vec{r}'))(\psi_i^{s''}(\vec{r}')[n^{s'}])^* \}d^3\vec{r}'.$$

And further with 8., 4., and

$$\frac{\delta \int |\psi_i^{s''}(\vec{r}')[n^{s'}]|^2 d^3\vec{r}'}{\delta n}(\vec{r}) = 0$$

(because of the normalization conditions

$$\int |\psi_i^{s''}(\vec{r})[n^{s'} + \delta n^{s'}]|^2 d^3\vec{r} = \int |\psi_i^{s''}(\vec{r})[n^{s'}]|^2 d^3\vec{r} = 1) \text{ this reduces to}$$

$$-\sum_{s''} q \int \mathcal{V}_{eff}^{s''}(\vec{r}') \frac{\delta \sum_i |\psi_i^{s''}(\vec{r}')[n^{s'}]|^2}{\delta n^s}(\vec{r}) d^3\vec{r}'.$$

But with $\sum_i |\psi_i^{s''}[n^{s'}](\vec{r})|^2 = n^{s''}(\vec{r})$ and 7. one gets

$$-\sum_{s''} q \int \mathcal{V}_{eff}^{s''}(\vec{r}') \frac{\delta \sum_i |\psi_i^{s''}(\vec{r}')[n^{s'}]|^2}{\delta n^s}(\vec{r}) d^3\vec{r}' =$$

$$-\sum_{s''} q \int V_{eff}^{s''}(\vec{r}') \delta_{s,s''} \delta(\vec{r} - \vec{r}') d^3\vec{r}' =$$

$$-q \mathcal{V}_{eff}^s(\vec{r}). \tag{2.8}$$

Finally (2.7) turns into:

$$\mu^s = -q\mathcal{V}_{eff}^s(\vec{r}) + qV^s(\vec{r}) + q^2 \int \frac{n(\vec{r})}{|\vec{r} - \vec{r}'|} d^3\vec{r}' + \frac{\delta E_{xc}[n^{s'}]}{\delta n^s}(\vec{r}).$$

This defines $\mathcal{V}_{eff}^s(\vec{r})$ up to a constant. If one assumes that V^s is already normalized, i.e. $V^s(\infty) = 0$, and furthermore that all charges are confined within a large sphere, which yields $\text{limit}_{r \to \infty} \int \frac{n(\vec{r})}{|\vec{r} - \vec{r}'|} d^3\vec{r}' = 0$, one gets with the definition $\mu_{xc}^s := \text{limit}_{r \to \infty} \frac{\delta E_{xc}[n^{s'}]}{\delta n^s}(\vec{r})$ and the fact that μ^s is a constant (see above):

$$\mathcal{V}_\infty^s = \frac{\mu_{xc}^s - \mu^s}{q}.$$

So the properly normalized effective potential is:

$$\mathcal{V}_{eff}^s(\vec{r}) = V^s(\vec{r}) + q \int \frac{n(\vec{r}')}{|\vec{r} - \vec{r}'|} d^3\vec{r}' + \frac{1}{q} \frac{\delta E_{xc}[n^{s'}]}{\delta n^s}(\vec{r}) - \frac{1}{q} \mu_{xc}^s. \tag{2.9}$$

which is the required formula.

2.2. A First Look at the KS Equations

Inserting equation (2.9) into (2.3) gives

$$[-\frac{\hbar^2}{2m}\vec{\nabla}^2 + qV^s(\vec{r}) + q^2 \int \frac{n(\vec{r})}{|\vec{r}-\vec{r}'|}d^3\vec{r}' + \frac{\delta E_{xc}[n^{s'}]}{\delta n^s}(\vec{r}) - \mu_{xc}^s]\psi_i^s(\vec{r}) = E_i^s\psi_i^s(\vec{r}), \quad (2.10)$$

with $n^s(\vec{r})$ given by (2.4).

These equations are non-linear integro-differential equations. It is impossible to solve them analytically. They are similar to the Hatree-Fock (HF) equations, which are derived for single Slater-determinant states in Fock-Space. The only difference is that the HF equations contain instead of $\frac{\delta E_{xc}[n^{s'}]}{\delta n^s}(\vec{r})$ a term $V_x(\vec{r})$ given, not only in terms of the density, but in terms of wave functions. As a result the KS equations are simpler. This term is called the exchange potential. The difference in the KS potential and the HF potential is called correlation (and thus includes effects that stem from linear combinations of Slater-determinants).

Figure 2.1 shows how to solve the KS equations iteratively. This procedure is called a self-consistent loop. The net effect of each step of the loop is to compute the new density from the old density by the steps given in the diagram. Clearly each step defines an operator $\mathcal{O}$ on the set of densities.

It is commonly assumed that the self-consistent algorithm converges, i.e. one always reaches the end of the loop and the result is unique. It turns out that the algorithm has to be slightly modified in order to ensure convergence (see below). A point that is not always discussed in the literature is to ensure that the operator $\mathcal{O}$ is well defined. i.e. is independent of which orthonormal basis (ONB) of H_{eff} is used to solve the KS equations. It can be easily proven, however, that $\mathcal{O}$ is indeed well-defined if one ignores the technical difficulty that the scattered states are not normalizeable.
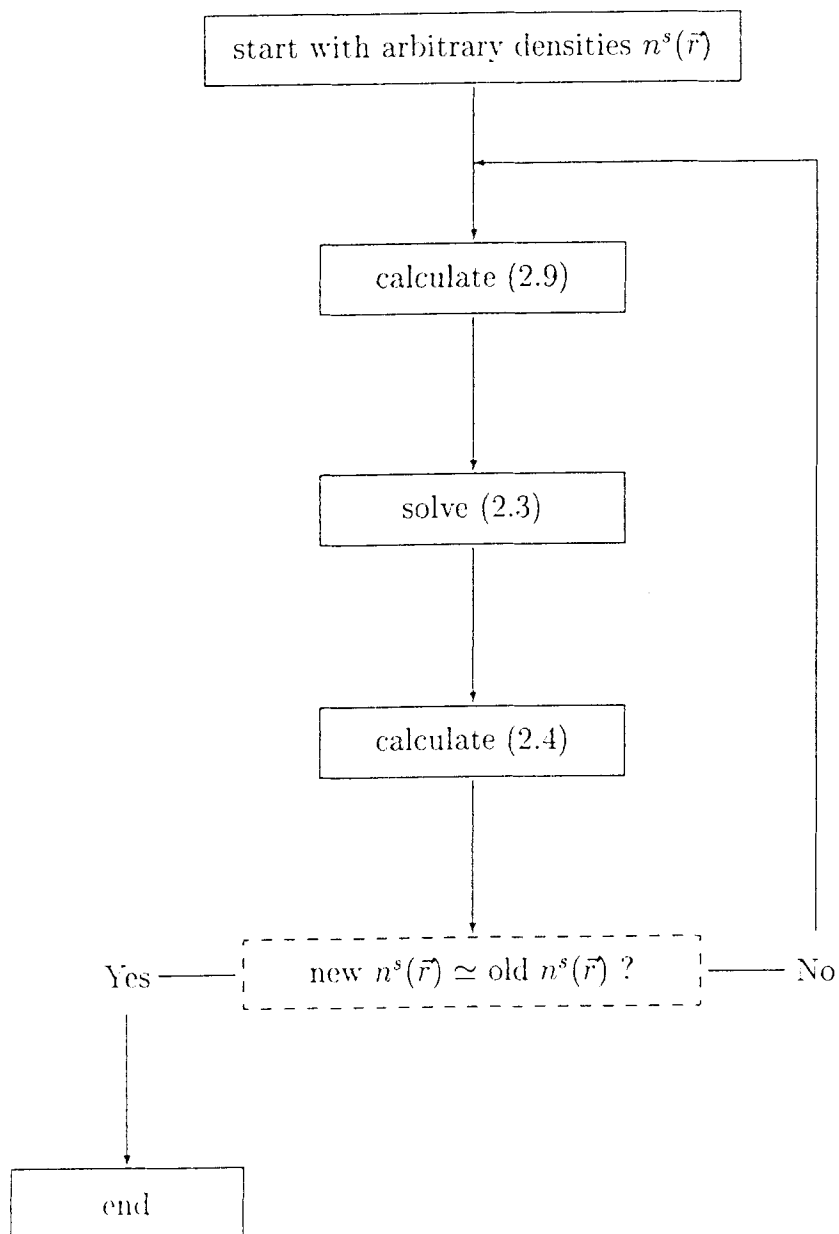
FIGURE 2.1. Flow diagram for the self-consistency equations

Let's assume that all states with energy smaller than μ are occupied and all other states are not. Let $\mathrm{Sub}(E \leq \mu)$ be the subspace of all occupied states. The Hamiltonian H_{eff} can be restricted to $\mathrm{Sub}(E \leq \mu)$, since $H_{eff}(\mathrm{Sub}(E \leq \mu)) \subseteq \mathrm{Sub}(E \leq \mu)$ (one can see this by choosing a basis of H_{eff}-eigenstates with $E \leq \mu$). Let $\{\psi_i^s(\vec{r})\}$ and $\{\phi_j^s(\vec{r})\}$ be two different ONBs of H_{eff}-eigenstates for $\mathrm{Sub}(E \leq \mu)$. All that has to be shown is, that these ONBs lead to the same density.

Since $\{\psi_i^s(\vec{r})\}$ and $\{\phi_j^s(\vec{r})\}$ are both complete within $\mathrm{Sub}(E \leq \mu)$ one can expand $\psi_i^s(\vec{r}) = \sum_j a_{i,j} \phi_j^s(\vec{r})$ and $\phi_j^s(\vec{r}) = \sum_i b_{j,i} \psi_i^s(\vec{r})$, where the condition that both $\{\psi_i^s(\vec{r})\}$ and $\{\phi_j^s(\vec{r})\}$ are orthonormal requires

$\sum_k a_{j,k}^* a_{i,k} = \delta_{j,i}$, $\sum_k b_{j,k}^* b_{i,k} = \delta_{j,i}$, and $b_{j,i} = a_{i,j}^*$ from which follows that

$\sum_l a_{l,k}^* a_{l,i} = \delta_{l,i}$.

Calculating the density gives

$$n^s(\vec{r}) = \sum_i |\psi_i^s(\vec{r})|^2$$
$$= \sum_i \left(\sum_k a_{i,k} \phi_k^s(\vec{r})\right)^* \left(\sum_l a_{i,l} \phi_l^s(\vec{r})\right)$$
$$= \sum_{k,l} \left(\sum_i a_{i,k}^* a_{i,l}\right) (\phi_k^s(\vec{r}))^* \phi_l^s(\vec{r})$$
$$= \sum_{k,l} \delta_{k,l} (\phi_k^s(\vec{r}))^* \phi_l^s(\vec{r}) = \sum_k |\phi_k^s(\vec{r})|^2.$$

This shows the independence.

Finally, if the end of the loop is reached the problem is solved, because the density to create the effective potential is the same as the density calculated from the effective potential.

2.3. Symmetry of the KS Equations

The complexity of the KS equations can be reduced by considering their symmetry properties. Impurity atoms which have not more than one partially filled angular momentum shell, have just one magnetic axis after symmetry breaking. So there is a symmetry direction given by this axis. For this reason it is justified to focus on axially symmetric starting densities. We use the self-consistency algorithm to prove the following theorem:

If one starts with a Φ-symmetric density and $V^s(\vec{r}) = V^s(r, \theta)$ (esp. $V^s(\vec{r}) = V^s(r)$, i.e. the external potential is spherically symmetric), then the density is Φ-symmetric for each iteration step.

The proof is by complete induction over the iteration steps.
For the first iteration step the assertion is satisfied since it was assumed that we start with a Φ-symmetric density.
The next thing is to prove that provided the density is Φ-symmetric for one iteration step, it has the same property for the next step.
Let

$$L_z = \frac{\hbar}{i} \frac{\partial}{\partial \Phi}$$

and

$$\mathcal{H}_{eff} = -\frac{\hbar^2}{2m_0} \vec{\nabla}^2 + q[V^s(r) + q \int \frac{n(\vec{r'})}{|\vec{r} - \vec{r'}|} d^3\vec{r'} + \frac{1}{q} \frac{\delta E_{xc}[n^{s'}]}{\delta n^s}(\vec{r})].$$

where the exchange energy E_{xc} is in most approximations an integral over some function of the density. Here it is only important that it does not depend on Φ if the density does not depend on Φ, which is satisfied for these E_{xc} models. Since the density $n(\vec{r})$ is assumed to be Φ-independent, so is $q \int \frac{n(\vec{r'})}{|\vec{r}-\vec{r'}|} d^3\vec{r'}$. Together with the assumption that $V^s(\vec{r})$ is Φ-independent it follows that also $\mathcal{H}_{eff}$ is Φ-independent.

or equivalently $[\mathcal{H}_{eff}, L_z] = 0$. As a well-known consequence one can choose eigenfunctions of $\mathcal{H}_{eff}$ of the form

$$\psi_{j,m}(r, \theta, \Phi) = R_{j,m}(r, \theta) \frac{1}{\sqrt{2\pi}} e^{im\Phi},$$

where m is the magnetic quantum number and j is a collection of all other quantum numbers (due to the fact that $\mathcal{O}$ is well-defined the theorem does not depend on this particular choice of eigenfunctions). Calculating the density for the next iteration step with these $\psi_{j,m}$ leads to:

$$n(r, \theta, \Phi) = \sum_{j,m} |R_{j,m}(r, \theta) \frac{1}{\sqrt{2\pi}} e^{im\Phi}|^2 = \frac{1}{2\pi} \sum_{j,m} |R_{j,m}(r, \theta)|^2.$$

This new density does not depend on Φ and thus the proof is complete.

It follows easily that even $\lim_{\text{iterations} \to \infty} n(r, \theta, \Phi)$ does not depend on Φ. Furthermore if one assumes that this limit, i.e. the solution to the whole problem, does not depend on the starting density one concludes:

The density that solves the KS equations is Φ-symmetric for a spherically symmetric external potential.

2.4. Bound and Scattered States

Rewriting (2.3) in the form

$$\vec{\nabla}^2 c_i^s(\vec{r}) = \frac{2m_0}{\hbar^2} [q\mathcal{V}_{eff}^s(\vec{r}) - E_i^s] c_i^s(\vec{r}),$$

suggests that for $q\mathcal{V}_{eff}^s(\infty) - E_i^s > 0$ one gets bound states, because in our case for some large enough $\mathcal{R}$ we have $q\mathcal{V}_{eff}^s(\vec{r}) - E_i^s > 0$ for all $r > \mathcal{R}$. Hence one gets a positive curvature-factor for c_i^s for all $r > \mathcal{R}$. As a result c_i^s behaves like a exponential function, i.e. falls off rapidly for increasing r. One gets a bound state indeed.

Conversely if $qV_{eff}^s(\infty) - E_i^s < 0$, one obtains by the same reasoning a negative curvature-factor for all large enough r. The asymptotic behavior in this case is like a sine function, i.e. the solution is not confined to a region around the scatterer. One gets scattered states.

In section 2.1 we already introduced the proper normalization of V_{eff}^s, namely $V_{eff}^s(\infty) = 0$. The conditions for having bound and scattered states are in this case of course, $E_i^s < 0$ and $E_i^s > 0$, respectively.

A more detailed argumentation can be found in the standard literature on Quantum Mechanics. It is also shown there that for $E_i^s < 0$ there is a discrete spectrum, whereas for $E_i^s > 0$ there is a quasi-continuous spectrum or a discrete spectrum depending on the boundary conditions.

Numerical methods to find the discrete eigenvalues E_i^s and the corresponding states do exist (see below). The scattered states require some extra theoretical consideration. The potential in $\mathcal{H}_{eff}$ shows screening effects after a few iteration steps. Consequently, one can assume that the potential behaves like a Yukawa-potential. This means it falls of fast enough to be approximated by $V_{eff}^s(\vec{r}) \approx 0$ for $r > R$, where R has to be large enough. Thus the Hamiltonian for the scattered states can be approximated by

$H_{scatt} = \mathcal{H}_{eff}$ for $r \leq R$ and $H_{scatt} = H_{free}$ for $r > R$, where H_{free} is the free particle Hamilonian. This suggests to approximate the energy of the scattered particle $E \approx E_{free} = \frac{\hbar^2 k^2}{2m}$ and expand the eigenstates in terms of the spherical harmonics $Y_{l,m}$, because l and m are good quantum numbers for H_{free}, since $[L^2, H_{free}] = [L_z, H_{free}] = 0$. This procedure is derived in detail in the next section.

2.5. Phase Shifts for Non-Spherical Potentials

The question of finding the scattered states is reduced to the question of finding phase shifts. As proven in section 2.3, it is for the purpose of this thesis sufficient to consider potentials of the form $V^s(r, \theta)$, i.e. Φ-symmetric potentials. Following the procedure indicated in section 2.4 one has to solve the following Schroedinger-equation in spherical coordinates:

$$[-\frac{\hbar^2}{2m_0}(\frac{2}{r}\frac{\partial}{\partial r} + \frac{\partial^2}{\partial r^2} + \frac{1}{r^2 \sin\theta}\frac{\partial}{\partial\theta}(\sin\theta\frac{\partial}{\partial\theta}) + \frac{1}{r^2 \sin\theta}\frac{\partial^2}{\partial\Phi^2}) +$$
$$V^s(r,\theta)]\psi(r,\theta,\Phi) = E\psi(r,\theta,\Phi) \qquad (2.11)$$

for $r \leq R$ and

$$-\frac{\hbar^2}{2m_0}(\frac{2}{r}\frac{\partial}{\partial r} + \frac{\partial^2}{\partial r^2} + \frac{1}{r^2 \sin\theta}\frac{\partial}{\partial\theta}(\sin\theta\frac{\partial}{\partial\theta}) + \frac{1}{r^2 \sin\theta}\frac{\partial^2}{\partial\Phi^2})\psi(r,\theta,\Phi) = E\psi(r,\theta,\Phi)$$

$$(2.12)$$

for $r > R$, where ψ has to be twice differentiable at $r = R$. The solutions for $r > R$ are as mentioned in the previous section

$$\psi^s_{i,l,m}(r,\theta,\Phi) = R^s_{i,l,m}(r)Y_{l,m}(\theta,\Phi) \qquad (2.13)$$

with

$$-\frac{\hbar^2}{2m_0}(\frac{2}{r}\frac{\partial}{\partial r} + \frac{\partial^2}{\partial r^2} - \frac{l(l+1)}{r^2})R^s_{i,l,m}(r) = ER^s_{i,l,m}(r),$$

where m is the magnetic quantum number, l is the angular momentum, s the magnetic spin quantum number, and i is a collection of all other quantum numbers. The solutions to the last equations are well-known:

$$R^s_{k,l,m}(r) = A^s_{k,l,m}j_l(kr) + B^s_{k,l,m}n_l(kr), \qquad (2.14)$$

where j_l and n_l are the spherical Bessel functions of the first and second kind respectively and since $E > 0$ one defines $E = \frac{\hbar^2 k^2}{2m}$. (The remaining quantum numbers i now turned out to be just k.) To match the solutions at $r \leq R$ and $r > R$ it is necessary to expand (since the $Y_{l,m}(\theta, \Phi)$ are a complete set of functions) the inside solution

$$\psi^s_{k,l,m}(r, \theta, \Phi) = \sum_{l'} R^{s,l}_{k,l',m}(r) Y_{l',m}(\theta, \Phi). \tag{2.15}$$

Note that m is, as pointed out in sec. 1.3, still a good quantum number and so there is no m-sum. Furthermore the subscript l referres to the l-value of the outside solution to which the inside solution is matched, whereas l' is just a summation subscript.

Inserting this into the Schroedinger equation for $r \leq R$ gives equations for the functions $R^{s,l}_{k,l',m}(r)$:

$$\sum_{l'} [-\frac{\hbar^2}{2m_0}(\frac{2}{r}\frac{\partial}{\partial r} + \frac{\partial^2}{\partial r^2} - \frac{l'(l'+1)}{r^2}) + V^s(r, \theta)] R^{s,l}_{k,l',m}(r) Y_{l',m}(\theta, \Phi)$$

$$= \frac{\hbar^2 k^2}{2m_0} \sum_{l'} R^{s,l}_{k,l',m}(r) Y_{l',m}(\theta, \Phi). \tag{2.16}$$

Multiplying these equations by $Y^*_{l'',m}(\theta, \Phi) \sin \theta$ and integrating $\int_0^\pi d\theta \int_0^{2\pi} d\Phi$ gives after using $\int_0^\pi \int_0^{2\pi} d\theta d\Phi \sin \theta Y^*_{l'',m}(\theta, \Phi) Y_{l',m}(\theta, \Phi) = \delta_{l',l''}$:

$$[-\frac{\hbar^2}{2m_0}(\frac{2}{r}\frac{\partial}{\partial r} + \frac{\partial^2}{\partial r^2} + \frac{l'(l'+1)}{r^2})] R^{s,l}_{k,l',m}(r) +$$

$$\sum_{l''} V^{s,m}_{l',l''}(r) R^{s,l}_{k,l'',m}(r) = \frac{\hbar^2 k^2}{2m_0} R^{s,l}_{k,l',m}(r). \tag{2.17}$$

where $V^{s,m}_{l',l''}(r) = \int_0^\pi \int_0^{2\pi} d\theta d\Phi \sin \theta Y^*_{l',m}(\theta, \Phi) V^s(r, \theta) Y_{l'',m}(\theta, \Phi)$. The fact that $V(r, \theta)$ does not depend on Φ leads to a simplification of these coefficients and to the important fact that they are real. This can be easily seen by using the definitions of the $Y_{l,m}(\theta, \Phi) = \sqrt{\frac{2l+1}{4\pi} \frac{(l-m)!}{(l+m)!}} P^m_l(\cos \theta) e^{im\phi}$ and $\int_0^{2\pi} (e^{im'\phi})^* e^{im\phi} d\phi = 2\pi \delta_{m,m'}$:

$$V_{l'',l'}^{s,m}(r) = \frac{1}{2}\sqrt{(2l''+1)\frac{(l''-m)!}{(l''+m)!}}\sqrt{(2l'+1)\frac{(l'-m)!}{(l'+m)!}} \cdot$$
$$\int_0^\pi d\theta \sin\theta P_{l''}^m(\cos\theta)V^s(r,\theta)P_{l'}^m(\cos\theta) \qquad (2.18)$$

From this equation it can be seen that they are indeed real, since $V^s(r,\theta)$ and $P_l^m(\cos\theta)$ are real functions. The fact that these coefficients are real allows us to look for real solutions $R_{k,l',m}^{s,l}(r)$ only.

The constraint that the overall solution has to be twice differentiable requires that the inside and outside solutions match at $r = R$ in the following sense (this can easily seen from (2.13) and (2.15)):

$R_{k,l',m}^{s,l}(R) = R_{k,l',m}^{'s,l}(R) = 0$ for $l' \neq l$ and

$R_{k,l,m}^{s,l}(R) = A_{k,l,m}^s j_l(kR) + B_{k,l,m}^s n_l(kR),$

$R_{k,l,m}^{'s,l}(R) = A_{k,l,m}^s k j_l'(kR) + B_{k,l,m}^s k n_l'(kR)$ for $l' = l$.

The first two equations impose boundary conditions on (2.17), the latter determine the coefficients $A_{k,l,m}^s$ and $B_{k,l,m}^s$.

To solve (2.17) uniquely additional boundary conditions, namely boundary conditions on $R_{k,l,m}^{s,l}$ and $R_{k,l,m}^{'s,l}$, are required. This is deferred to a later chapter for the spherically symmetric case; the purpose of this section is to define phase shifts. Here it is only important to know that (2.17) with the appropriate boundary conditions can be solved uniquely.

As already mentioned, once (2.17) is solved, $A_{k,l,m}^s$ and $B_{k,l,m}^s$ can be determined. The fact that $R_{k,l',m}^{s,l}(r)$, $j_l(kr)$, and $n_l(kr)$ are real leads to real coefficients $A_{k,l,m}^s$ and $B_{k,l,m}^s$ in (2.14). Thus it is possible to generalize the definition of phase shifts (see e.g. [4, eqn. (11.46)]) to

$$\tan\delta_{k,l,m}^s = -\frac{B_{k,l,m}^s}{A_{k,l,m}^s}$$

To make the continuous k-dependence more explicit the phase shift is referred to as $\delta^s_{l,m}(k)$ in the following .

The origin of the name 'phase shift' can be seen by comparing the radial solution of the free Hamiltonian and the solution of the scattered Hamiltonian for large r: The first one is

$$j_l(kr) \rightarrow \frac{1}{kr} \sin(kr - \frac{l\pi}{2}), \qquad (2.19)$$

since $n_l(kr)$ is not finite at $r = 0$, the latter one is

$$
\begin{aligned}
A^s_{k,l,m}[j_l(kr) &- \tan \delta^s_{l,m}(k) n_l(kr)] \rightarrow \\
A^s_{k,l,m} &\frac{1}{kr} [\sin(kr - \frac{l\pi}{2}) - \tan \delta^s_{l,m}(k) \cos(kr - \frac{l\pi}{2})] \\
= \frac{A^s_{k,l,m}}{kr \cos \delta^s_{l,m}(k)} &[\cos \delta^s_{l,m}(k) \sin(kr - \frac{l\pi}{2}) - \sin \delta^s_{l,m}(k) \cos(kr - \frac{l\pi}{2})] \\
&= \frac{A^s_{k,l,m}}{kr \cos \delta^s_{l,m}(k)} \sin(kr - \frac{l\pi}{2} + \delta^s_{l,m}(k)), \qquad (2.20)
\end{aligned}
$$

which shows that for large r the net effect (up to pre-factors) of the scattering center is to produce a phase shift $\delta^s_{l,m}(k)$ in the radial function.

2.6. Density of Induced States

The density of states of the continuous spectrum tells how many states are in an energy interval between E and $E + dE$ (or equivalently between k and $k + dk$, since $E = \frac{\hbar^2 k^2}{2m}$).

Once the phase shift is known the density of the scattered states can be obtained by the following reasoning, taken from [3]. Again the point of view is adopted that all charges are confined within a large sphere of radius $\mathcal{R}$. Therefore the boundary condition on the extended states is that they vanish at $r = \mathcal{R}$. Since the sphere

is large, the asymptotic values (2.19) and (2.20) can be used instead of the exact states. The boundary condition then becomes

$$kR - \frac{l\pi}{2} = n_{free}\pi$$

for the free states and

$$kR - \frac{l\pi}{2} + \delta^s_{l,m}(k) = n_{scatt}\pi$$

for the scattered states (n_{free} and n_{scatt} are natural numbers, that can be interpreted as the number of states between 0 and k). The number of partial states between $k \ldots k + dk$ is for the first case

$$\frac{dn_{free}}{dk}dk = \frac{R}{\pi}dk$$

and for the second case

$$\frac{dn_{scatt}}{dk}dk = \frac{R}{\pi}dk + \frac{1}{\pi}\frac{d\delta^s_{l,m}(k)}{dk}dk,$$

if k can be approximated as a continuous variable, which is justified for a large R. Subtracting the last two equations gives the additional states that are produced by the presence of a scattering center

$$\frac{d(n_{scatt} - n_{free})}{dk}dk = \frac{1}{\pi}\frac{d\delta^s_{l,m}(k)}{dk}dk.$$

To obtain the total additional spin states $d(\Delta N^s(k))$ between $k \ldots k + dk$ one has to sum

$$\frac{d(\Delta N^s(k))}{dk}dk = \frac{1}{\pi}\sum_{l,m}\frac{d\delta^s_{l,m}(k)}{dk}dk \qquad (2.21)$$

2.7. Immersion Energy

In order to obtain the electronic structure of a system, the methods of the previous sections are applied to fermions with charge $q = -e$, mass $m_0 = m_e$ and spin $S = \frac{1}{2}$. There are two spin-charge densities $n^{+\frac{1}{2}}(\vec{r})$ and $n^{-\frac{1}{2}}(\vec{r})$. These are abbreviated by $n^+(\vec{r})$ and $n^-(\vec{r})$, respectively.

The immersion energy E_{imm} of an impurity atom in jellium is defined as the energy of the impurity system E_{imp} minus the energy of its constituents, i.e. the energy of the pure jellium system E_{pure} plus the energy of the bare impurity atom E_{atom}:

$$E_{imm} = E_{imp} - E_{pure} - E_{atom}. \tag{2.22}$$

This energy can be calculated with the methods described in the previous sections. Some ideas are taken from [10]. It was not a part of this thesis to calculate E_{atom}. The data were provided by Dr. Jansen. In principle it can be calculated by setting the background density $n_0 = 0$ and sum over the bound states of the resulting KS equations.

The difference $E_{imp} - E_{pure}$ is calculated by separating this expression in kinetic energy, classical coulomb energy, and exchange-correlation energy:

$$E_{imp} - E_{pure} = \Delta T + \Delta C + \Delta E_{xc}.$$

- ΔC:

  Because of symmetry the electron density of the pure system is constant (if the system is large enough, when the boundaries can be ignored) and the Coulomb energy is zero. The Coulomb energy of the impurity system is:

$$\frac{1}{2}e^2 \int \int \frac{\{n_0 - n(\vec{r})\}\{n_0 - n(\vec{r}')\}}{|\vec{r} - \vec{r}'|} d^3\vec{r}\,d^3\vec{r}' + \int \frac{Ze}{r}e\{n_0 - n(\vec{r})\}d^3\vec{r},$$

where the last term is the potential energy due to the nucleus of the impurity atom. The homogeneous positive jellium background n_0 is the same. The integrals are taken over the volume of the system. One obtains:

$$\Delta C = e^2 \int \left(\frac{1}{2}\int \frac{n(\vec{r}') - n_0}{|\vec{r} - \vec{r}'|}d^3\vec{r}' - \frac{Z}{r}\right)\{n(\vec{r}) - n_0\}d^3\vec{r} \qquad (2.23)$$

- ΔT:

First we consider the difference of the kinetic energy for the bound states.

Of course, the pure system has no bound states and again there is no contribution of the pure system.

The kinetic energy of the bound states caused by the impurity atom can be calculated from (2.3):

$$\sum_{i,s}\{E_i^s + e\int \mathcal{V}_{eff}^s(\vec{r})|\psi_i^s(\vec{r})|^2 d^3\vec{r}\}$$

$$= \sum_{i,s} E_i^s + \sum_s e\int \mathcal{V}_{eff}^s(\vec{r})\sum_i |\psi_i^s(\vec{r})|^2 d^3\vec{r}$$

$$= \sum_{i,s} E_i^s + \sum_s e\int \mathcal{V}_{eff}^s(\vec{r})n_{bound}^s(\vec{r})d^3\vec{r},$$

where the sums are taken over all binding energies.

In the case of the extended states the impurity atom acts as a scattering center. It is assumed that the insertion of the impurity atom into the jellium does not change the Fermi-energies E_F^s of the system, what is justified for large systems (see below for more detailed argument). Then, of course, the

Fermi-wave-vectors $k_F^s = \frac{\sqrt{2m_e E_F^s}}{\hbar}$ do not change either.

Thus the it additional kinetic energy caused by the impurity atom is

$$\sum_s \left(\int_0^{k_F^s} \frac{\hbar^2 k^2}{2m_e} \frac{d(\Delta N^s(k))}{dk} dk + e \int \mathcal{V}_{eff}^s(\vec{r}) n_{scattered}^s(\vec{r}) d^3\vec{r} \right),$$

where $\frac{d(\Delta N^s(k))}{dk} dk$ is the number of states induced by the scatterer between $k \ldots k + dk$. But exactly this quantity was written in (2.21) in terms of phase shifts. Using this expression gives for the the first term of the kinetic energy difference due to the scattered states

$$\frac{1}{\pi} \sum_s \int_0^{k_F^s} \frac{\hbar^2 k^2}{2m_e} \sum_{l,m} \frac{d\delta_{l,m}^s(k)}{dk} dk,$$

or if the phase is viewed as a function of E due to the relation $k = \frac{\sqrt{2m_e E}}{\hbar}$

$$= \frac{1}{\pi} \sum_{s,l,m} \int_0^{E_F^s} E \frac{d\delta_{l,m}^s(E)}{dE} dE$$

$$= \frac{1}{\pi} \sum_{s,l,m} \left\{ E\delta_{l,m}^s(E)|_0^{E_F^s} - \int_0^{E_F^s} \delta_l^s(E) dE \right\}$$

$$= \frac{1}{\pi} \sum_{s,l,m} E_F^s \delta_{l,m}^s(E_F^s) - \frac{1}{\pi} \sum_{s,l,m} \int_0^{E_F^s} \delta_{l,m}^s(E) dE,$$

since the scattered states occupy the energies $0 \ldots E_F^s$ at T=0 [2]. Putting the contributions of the bound and scattered states together gives:

$$\Delta T = \sum_{i,s} E_i^s + \sum_s e \int \mathcal{V}_{eff}^s(\vec{r}) n^s(\vec{r}) d^3\vec{r} +$$

$$\frac{1}{\pi} \sum_{s,l,m} E_F^s \delta_{l,m}^s(E_F^s) - \frac{1}{\pi} \sum_{s,l,m} \int_0^{E_F^s} \delta_{l,m}^s(E) dE, \qquad (2.24)$$

since $n^s(\vec{r}) = n_{bound}^s(\vec{r}) + n_{scattered}^s(\vec{r})$.

---

[2]This is not a contradiction to Fumi's theorem [9, eqn. (4)], since this equation is derived for impurity ions, not atoms. If one adds $\sum_s E_F^s Z^s$ to Fumi's equation to take care of the energy required to add the extra Z electrons to the ion system and uses the Friedel sum rule $Z^s = \int_0^{E_F^s} \frac{d(\Delta N^s(E))}{dE} dE = \frac{1}{\pi} \sum_{l,m} \delta_{l,m}^s(E_F^s)$ one gets exactly the same result. This is in fact another way to derive the above expression.

- ΔE_{xc}:

  It was already discussed that the electron density of the pure system was uniform. The same is true for the spin-density states. They are called n_0^- and n_0^+ respectively. The exchange-correlation energy for the pure system is thus

  $$E_{cx}^{pure} = E_{xc}[n_0^-, n_0^+].$$

  The exchange energy for the impure system is

  $$E_{xc}^{impure} = E_{xc}[n^-, n^+],$$

  where now $n^-(\vec{r})$ and $n^+(\vec{r})$ have to be calculated from the states, that are solutions to the KS equations of the system.

  So

  $$\Delta E_{xc} = E_{xc}[n^-, n^+] - E_{xc}[n_0^-, n_0^+]. \tag{2.25}$$

Combining (2.23), (2.24), (2.25), and (2.22) leads to

$$\begin{aligned}
E_{imm} = \sum_{i,s} E_i^s + \sum_s e \int \mathcal{V}_{eff}^s(\vec{r}) n^s(\vec{r}) d^3\vec{r} - \\
\frac{1}{\pi} \sum_{s,l,m} E_F^s \delta_{l,m}^s(E_F^s) - \frac{1}{\pi} \sum_{s,l,m} \int_0^{E_F^s} \delta_{l,m}^s(E) dE + \\
e^2 \int \left(\frac{1}{2} \int \frac{n(\vec{r}') - n_0}{|\vec{r} - \vec{r}'|} d^3\vec{r}' - \frac{Z}{r} \right) (n(\vec{r}) - n_0) d^3\vec{r} + \\
E_{xc}[n^-, n^+] - E_{xc}[n_0^-, n_0^+] - E_{atom}
\end{aligned} \tag{2.26}$$

2.8. Exchange-Correlation Energy Models

Almost all exchange-correlation energy models are based on the local density approximation (LDA). In this approximation the exchange-correlation energy is written

$$E_{xc}[n^s] = \int \epsilon_{xc}(n^s(\vec{r}))n(\vec{r})d^3\vec{r}, \qquad (2.27)$$

where $\epsilon_{xc}(n^s)$ is the exchange-correlation energy density for a gas of uniform density n^s.

One might expect that this approximation is only valid for slowly-varying densities. It turns out, however, that the LDA is sufficient even for higher density gradients. The following is a brief overview of ϵ_{xc}-expressions for the electron gas.

2.8.1. Spin-Independent Models

There are two density regimes where analytical equations for $\epsilon_{xc}(n)$ can be obtained by perturbation theory (Feynman-graphs), namely for very low densities and for very high densities. The first expression is by Wigner

$$\epsilon_{xc}(n) = \frac{e^2}{a_0}\left(\frac{1}{1.105}r_S^2 - \frac{0.458}{r_S} - \frac{0.44}{r_S + 7.8}\right),$$

where $r_S = \left(\frac{3}{4\pi n}\right)^{\frac{1}{3}}\frac{1}{a_0}$ is the Wigner-Seitz radius. The second by Gell-Mann and Brueckner

$$\epsilon_{xc}(n) = \frac{e^2}{a_0}\left(-\frac{0.458}{r_S} - \frac{1}{n}(0.031\ln(r_S) - 0.047)\right)n.$$

The other common parameterizations are either interpolations or extrapolations of these two cases. These can be written as

$$\epsilon_{xc}(n) = \frac{e^2}{a_0}\left(-\frac{0.458}{r_S} - C \cdot G(\frac{r_S}{A})\right), \qquad (2.28)$$

where

$$G(x) = (1 + x^3)\ln(1 + \frac{1}{x}) - x^2 + \frac{x}{2} - \frac{1}{3}$$

and typical values for A and C are:

$A = 11.4\ C = 0.0333$ Gunnarsson-Lundquist (see [11])

$A = 21.0\ C = 0.0225$ Hedin-Lundquist

2.8.2. *Spin-Dependent Models*

One usually parameterizes in terms of the quantities

$n(\vec{r}) = n^-(\vec{r}) + n^+(\vec{r})$ and $\zeta(\vec{r}) = \frac{n^+(\vec{r}) - n^-(\vec{r})}{n(\vec{r})}$.

Most parameterizations are based on an interpolation between paramagnetic (unpolarized; $\zeta = 0$) and ferromagnetic (completely polarized; $|\zeta| = 1$) systems, i.e.

$$\epsilon_{xc}(n, \zeta) = f(\zeta)\epsilon_{xc}^{\zeta=0}(n) + (1 - f(\zeta))\epsilon_{xc}^{|\zeta|=1}(n), \tag{2.29}$$

where

$$f(\zeta) = \frac{(1 + \zeta)^{\frac{4}{3}} + (1 - \zeta)^{\frac{4}{3}} - 2}{2(2^{\frac{1}{3}} - 1)}$$

and $\epsilon_{xc}^{\zeta=0}$, $\epsilon_{xc}^{|\zeta|=1}$ are of the form (2.28) with the parameters A, C fitted for the appropriate polarization. So one has for example

$A^{\zeta=0} = 30.0 \quad C^{\zeta=0} = 0.0252$

$A^{|\zeta|=1} = 75.0 \quad C^{|\zeta|=1} = 0.0127$ Gunnarson-Lundquist

$A^{\zeta=0} = 11.4 \quad C^{\zeta=0} = 0.0333$

$A^{|\zeta|=1} = 15.9 \quad C^{|\zeta|=1} = 0.0203$ vonBarth-Hedin.

The parameterization used in this thesis is the Hedin-Lundquist form.

2.8.3. *Exchange-Correlation Potential*

Once the parameterization of the exchange-correlation energy is given, the exchange-correlation potential(s) $\frac{1}{e}\frac{\delta E_{xc}[n^-, n^+]}{\delta n^{\pm}}(\vec{r})$ are easily calculated by property 9 in sec. (2.1). The result is

$$\frac{1}{e}\frac{\delta E_{xc}[n^-, n^-]}{\delta n^-}(\vec{r}) = \frac{1}{e}\{\frac{\partial \epsilon_{xc}}{\partial n}(n(\vec{r}), \zeta(\vec{r})) + (1 - \zeta(\vec{r}))\frac{\partial \epsilon_{xc}}{\partial \zeta}(n(\vec{r}), \zeta(\vec{r}))\}$$

$$\frac{1}{e}\frac{\delta E_{xc}[n^-,n^+]}{\delta n^+}(\vec{r}) = \frac{1}{e}\{\frac{\partial \epsilon_{xc}}{\partial n}(n(\vec{r}),\zeta(\vec{r})) - (1 + \zeta(\vec{r}))\frac{\partial \epsilon_{xc}}{\partial \zeta}(n(\vec{r}),\zeta(\vec{r}))\}. \qquad (2.30)$$

For the spin independent model used in this thesis there is only one exchange cor-relation potential which is with (2.28):

$$\frac{1}{e}\frac{\delta E_{xc}[n]}{\delta n}(\vec{r}) = \frac{e}{a_0}(-\frac{4}{3}(\frac{0.458}{r_S} - C \cdot log(1 + \frac{A}{r_S})).$$

3. IMPLEMENTATION OF THE NUMERICS

In the remainder of this thesis Rydberg atomic units are used. These are defined by $\hbar^2 = 1$, $a_0 = 1$, and $2m_e = 1$. It follows that $e^2 = 2$ and that the energy unit $1 \; rmRy$ is the ionization energy of H (about 13.6eV).

3.1. Self-Consistency Loop

This chapter shows how to implement Fig. 2.1 on a computer. One starts with a suitable input density. In this thesis a superposition of the atomic density, which is calculated by another program, and the uniform background density is chosen. Then the initial effective potential is calculated. The Schroedinger equation is solved for the bound and extended states. The N energetically lowest states are populated, where N is the number of electrons in the system. From this the new density is calculated and also the final effective potential. So far everything is according to Fig. 2.1. But as already mentioned the algorithm has to be altered slightly in order to ensure convergence. This change affects the feedback.

Experience shows that if one takes the final effective potential of the previous iteration step as an initial effective potential for the new iteration step, the algorithm does not converge because the response of the system is too strong. One can deal with this problem by introducing a mixing ratio a ($0 < a < 1$) and taking $V_{eff}^{initial,i+1}(r) = aV_{eff}^{final,i}(r) + (1-a)V_{eff}^{initial,i}(r)$ (i indicates the iteration step) as a new initial potential. If one takes the mixing ration as low as 0.01 to 0.05 the algorithm indeed converges for most systems. The lower a is, however, the slower is the convergence. One idea to speed up the convergence is called Pratt's scheme. It is based on the idea of introducing an r-dependent mixing ratio, taking the last two iteration steps and interpolating for each r the points $(V_{eff}^{initial,i-1}(r), V_{eff}^{final,i-1}(r))$

and $(\mathcal{V}_{eff}^{initial,i}(r), \mathcal{V}_{eff}^{final,i}(r))$ to the line $\mathcal{V}_{eff}^{initial}(r) = \mathcal{V}_{eff}^{final}(r)$. This procedure leads to a mixing ratio of $a(r) = \dfrac{\mathcal{V}_{eff}^{initial,i-1}(r) - \mathcal{V}_{eff}^{initial,i}(r)}{\mathcal{V}_{eff}^{initial,i-1}(r) + \mathcal{V}_{eff}^{final,i}(r) - \mathcal{V}_{eff}^{initial,i}(r) - \mathcal{V}_{eff}^{final,i-1}(r)}$.

Since this procedure can give quite large or even negative mixing ratios, it is necessary to confine it to a minimum and a maximum value, typically 0 and 1 respectively. Whenever $a(r)$ is smaller than 0, it is set to 0, whenever it is larger than 1, it is set to 1. The problem with this procedure is that it can introduce discontinuities in the potential, when the mixing ratio suddenly switches from one r to the other from its minimum value to its maximum value or the other way around. One way around this is to smoothen out the transition by replacing $a(r)$ by $\dfrac{(min+max)a(r) - 2 \cdot min \cdot max}{2a(r) - (min+max)}$, where min and max are the minimal and maximal allowed values for the mixing respectively, whenever the old $a(r)$ is larger then max or smaller than min.

But this procedure leads to some peaks and wiggles in the potential and one often has to go back to a straight mixing ratio.

3.2. Simplifications and Approximations

The calculations were done spin-independently, i.e. equation (2.28) was used for the exchange-correlation energy with the parameter-set of Hedin-Lundquist. The extension to spin-dependent calculations is straight-forward and will be done in a future thesis.

Another simplification is to approximate equations (2.17). The problem is that these equations are coupled. But one can see by looking at the definition of the factors $V_{l',l''}^{s,m}(r)$ that they decouple for spherically symmetric potentials since $V_{l',l''}^{s,m}(r) = V^s(r)\delta_{l',l''}$ if V^s is θ-independent. To ensure a spherically symmetric potential for every iteration step in the self-consistency loop, it is necessary to assume

fully occupied l-shells. If this not the case one has to average over all different m-states within a shell. This is clearly an approximation if the number of electrons in the system is such that the outermost shell is not completely occupied. If one applies this averaging, however, it can be shown by the same means as in section 2.3 that an initially spherically symmetric potential leads to spherically symmetric densities for all iteration steps. Since the radial equations (2.17) are not m-dependent anymore, the idea is to expand the eigenfunction in terms of $Y_{l,m}(\theta, \Phi)$ and sum over all m-values using $\sum_{m=-l}^{l} |Y_{l,m}(\theta, \Phi)|^2 = \frac{2l+1}{4\pi}$, which says that the average is indeed spherically symmetric.

A further results of spherical symmetry is that the phase shifts are also m-independent.

In the following development only spherically averaged systems are considered.

3.3. The Question of Boundary Conditions

The suitable choice of boundary conditions for a spherically symmetric potential are spherically symmetric boundary conditions. Therefore we use a model in which all charges are contained in a sphere of radius $\mathcal{R}$ with the impurity atom at the center; the charge density is zero outside. Then the boundary condition on the wave-functions are that they have to vanish at $r = \mathcal{R}$.

The reason for the choice of these boundary conditions is a purely practical one. The calculated quantities should not depend on the boundary conditions. To test this two different choices for $\mathcal{R}$ were implemented. They reflect the two extreme cases. The first one is to set $\mathcal{R}$ to its minimal possible value, i.e. the cutoff-radius R_c beyond which the potential is zero, the second to let $\mathcal{R}$ approach to infinity. The results should be about the same for both cases.

In case one the number of electrons in the sphere is fixed at the value $Z + n_0 \cdot \frac{4\pi}{3} R_c^3$ by the boundary conditions. In case two the number of available electrons is potentially infinite and so there is no restriction on the number of electrons in a sphere of radius R_c. The system is determined by a fixed Fermi-level $E_F = 9\pi^{\frac{4}{3}} \cdot n_0^{\frac{2}{3}}$.

The following development in this chapter distinguishes between these different boundary conditions.

3.4. Bound State Search

The idea of how to search for the energy eigenvalues is taken from [7, p. 139]. The procedure is the following:

One can characterize the radial function of a bound state uniquely by its angular momentum l and its number of nodes n_{nodes} since the number of nodes for two different bound states with the same l has to be different because of orthogonality. Instead of using $|n_{nodes}, l >$ as a label one often uses $|n, l >$, where $n = n_{nodes} + l + 1$ is the principal quantum number. From $n_{nodes} \geq 0$ it that follows $l = 0 \ldots n - 1$. The bound state search was stopped when there was no bound state found for a certain principal quantum number.

One knows that the energy of a state $|n, l >$ in a pure Coulomb potential is $-\frac{Z^2}{n^2} Ry$, where Z is the charge of the impurity atom. The potentials we consider here are screened Coulomb potentials, so the corresponding energy eigenvalues for a state with the same quantum numbers would be higher than for a bare Coulomb potential. An upper boundary for the energy eigenvalues is 0, since we are dealing with bound states.

To find the bound state energies one guesses an initial energy eigenvalue for a state $|n, l >$ within $[-\frac{Z^2}{n^2} Ry, 0]$. With this energy value one starts to integrate

the Schroedinger equation from an inner cut-off radius r_c close to the origin outwards and from the outer cut-off radius R_c inwards to a matching point (for which we chose the innermost classical turning point). The limiting values at the origin are given by $\psi_{E,l}(r) = r^l$ and $\psi'_{E,l}(r) = l r^{(l-1)}$ for all potentials that do not diverge faster than $\frac{1}{r}$ at the origin. One can use these limiting values as boundary values for the outward integration. The boundary values at the outer cut-off radius depend on the radius $\mathcal{R}$. For the first case considered, where $\mathcal{R} = R_c$, one simply starts the inward integration with $\psi_l(R_c) = 0$ and an arbitrary value for $\psi'_l(R_c)$ (this value factors out when one matches the inner and outer solutions, because of the linearity of the Schroedinger equation; a suitable value would be the same as for the next case). For the second case, where $\mathcal{R}$ goes to infinity one can use asymptotic values

$$\psi_{E,l}(r) = \frac{e^{(-\sqrt{-E}r)}}{r} \quad \text{and} \quad \psi'_{E,l}(r) = \frac{-\sqrt{-E}\, e^{(-\sqrt{-E}r)}}{r} - e^{(-\sqrt{-E})},$$

which are valid when potential and centrifugal potential can be neglected, to determine the boundary values at the outer cut-off radius. (If the energy is very low it is sometimes necessary to start the integration from farther inside, in order to prevent an underflow. A good criteria for double precision numbers is $\sqrt{-E}r < 36$.) Then one re-scales the outer solution to match the inner solution at the innermost classical turning point for the total potential and energy. For numerical reasons it is the best choice to take the innermost classical turning point as a matching point, because the other turning points might appear and disappear as the potential changes for different iteration steps. The reason for taking a turning point as a matching point is that at the turning point the inner solution changes its behavior from oscillatory to exponential-like. By integrating beyond the turning point, one would pick up a solution that blows up exponentially.

In order to get a solution to the differential equation the first derivatives also have

to match at the turning point. This happens only for the correct energy value. So the difference in first derivatives of the inward and outward solutions at the turning point indicates if the energy guess was too high or too low. Fig. 3.1 is a plot of this difference in derivatives multiplied by the sign of the wave functions at the turning point for the hydrogen atom with $l = 0$. One can see that difference is indeed zero for the right energy values $-\frac{1}{n^2}$ Ry. The large discontinuities in this plot are where the number of nodes of the wave function changes. (The small discontinuities are caused when the turning point changes.) One can also see that the difference is larger than zero if the guessed energy value E leads to the right number of nodes, but is too small, and that the difference is negative, if the E is too large.

To decide if there is a bound state between a certain energy minimum and a certain energy maximum one has to check the number of nodes and the difference in first derivatives at the turning point. (Sometimes the initial energy guess for the minimum energy was to low to have a turning point. In this case the minimum energy was increased by small steps until a turning point was found.) If the number of nodes for the minimum energy is greater than the number of the required nodes or the number of nodes for the maximum energy is less then the number of required nodes there is no bound state within the given interval, since greater energies correspond to a greater number of nodes. Furthermore, if the number of nodes for the minimum energy and the number of nodes for the maximum energy are the same and the difference in first derivatives at the turning point is negative for the minimum energy or positive for the maximum energy, there is also no bound state in the given interval. Otherwise there is a bound state. One can find its energy to any desired precision by implementing a bisection algorithm.

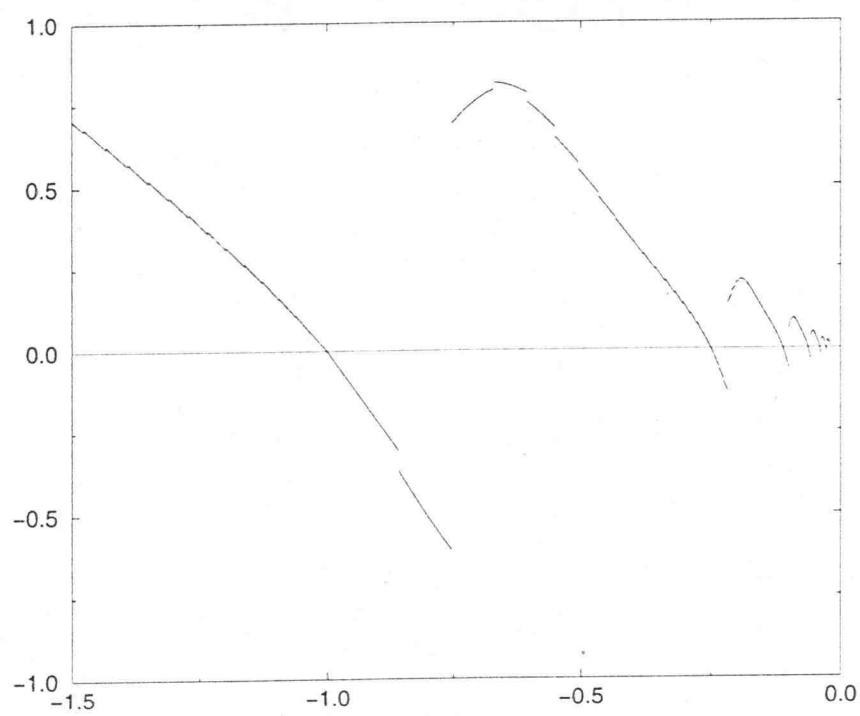After the energy and states are found they are normalized to unity within the sphere.

FIGURE 3.1. Difference in derivatives at the classical turning point vs. E

3.5. Determination of the Scattered States

The procedure to find the scattered states is very different for the two kinds of boundary conditions. The first case discussed is the one with finite $\mathcal{R}$.

In this case the procedure is straight forward. The states can also be labeled by their number of nodes within the sphere and the angular momentum. One takes a mesh in k-space (which is one-dimensional for spherically symmetric potentials) and integrates outwards starting from the inner cut-off using the same limiting values as for the bound states. If two adjacent k-points give wave functions with different signs at the end point $r = R_c$, there has to be a k-point between them, which gives a node of the wave function at the end point. This k-value can be found by a linear interpolation of the previous two k-points and gives a state with the right boundary conditions $\psi(R_c) = 0$. (The values of the states at R_c obtained by this method were mostly better than $10^{(-3)}$.) Again this state can be normalized within the sphere. Since the energy is k^2, the lower energy states are automatically found first by this search algorithm.

This is illustrated in Fig. 3.2, where the value of the wave-function at the endpoint R_c versus different k-values is plotted. Whenever the graph intersects zero, a states is found. The very sharp transition for the first state occurs only for $l = 0$ and if there are very large oscillations in the effective potential. They are also the reason for numerical errors, since the state cannot be determined exactly enough.

The scattered state search can be limited to a maximal l-value of kR_c, where R_c is the cut-off radius for the potential, for the following reason:

According to eqn. [5. C-48] the states for a potential with a cut-off radius and with l-values, that satisfy $\sqrt{l(l+1)} \geq kR_c$, are approximately equal to the free states
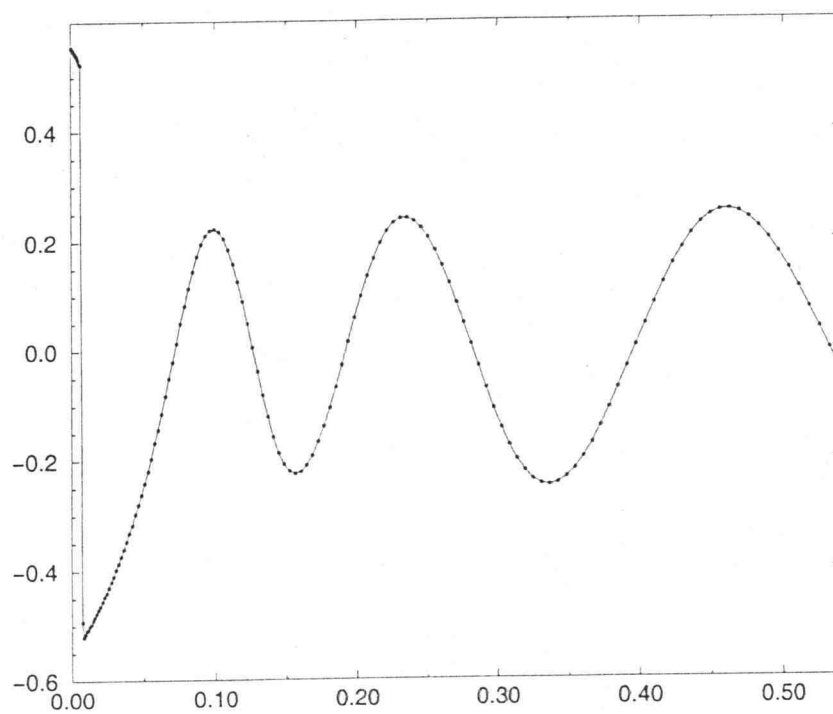
FIGURE 3.2. $\psi_{k,l}(R_c)$ vs. k for $l = 0$

with the same l-value (since in this case j_l is small where the potential is large and vice versa; so their product is always small). But one knows from [3, p. 233] that the k-values for the free states are given by $k = \frac{\pi}{\mathcal{R}}(n + \frac{l}{2})$ or, solving for l: $l = \frac{2(k\mathcal{R}-n)}{\pi}$. Since n is larger or equal to 1, the maximal l-value for a given k-value is $l = \frac{2(k\mathcal{R}-1)}{\pi}$. For $\mathcal{R} = R_c$ an upper boundary for l that satisfies both $\sqrt{l(l+1)} > kR_c$ and $l > \frac{2(k\mathcal{R}-1)}{\pi}$ is for example $l = k\mathcal{R}$. Beyond this l-value one can stop the state search.

In the second case, where $\mathcal{R}$ goes to infinity, the situation is completely different than for the bound states and the scattered states for the finite sphere. First the number of nodes will be infinite for all states, because of the oscillatory behavior and the infinite radius. Furthermore, there is no k-quantization anymore, because of the lack of boundary conditions. So all k-values up to the Fermi level are possible. The Fermi wave vector for a free electron gas can be found in any textbook on solid state physics and is given by $k_F^3 = 3\pi^2 n_0$, where n_0 is the (uniform) electron density. It is assumed that this relation also holds for the impurity system, if the dimension of the system are much larger than the dimensions of the impurity atom. The reason is that the Fermi-energy is equal to the chemical potential at $T = 0$, which is the energy required to put an electron into the system. This number does not change compared to the uniform gas if the effect of the atomic potential at the surface of the system can be neglected.

The task is now to calculate the Friedel oscillations. One expands the uniform background density in terms of the solutions of the free electron system using [8, 10.1.50] $\sum_l (2l+1) j_l^2(kr) = 1$ and $\int_0^{k_F} k^2 dk = \frac{1}{3} k_F^3 = \pi^2 n_0$. Multiplying the last two equations together and rearranging some terms gives $n_0 = \frac{1}{\pi^2} \int_0^{k_F} \sum_l (2l + 1) k^2 j_l^2(kr) dk$. One expands the density of the impurity system by replacing $j_l(kr)$ by the radial solutions

$R_{k,l}(r)$ of the Schroedinger equation. The normalization of those have to be such that they have the same asymptotic behavior as $j_l(kr) \to \frac{1}{kr}\sin(kr - \frac{l\pi}{2})$, namely they have to be fit to $j_l(kr)\cos\delta_l(k) - n_l(kr)\sin\delta_l(k) \to \frac{1}{kr}\sin(kr - \frac{l\pi}{2} + \delta_l(k))$ at the cut-off radius R_c (This normalization also implies that $R_{k,l}(r) \to j_l(kr)$ for $r > R_c$ if $\delta_l(k) \to 0$). This works for $\mathcal{R} \to \infty$, since the density of states $\frac{dn}{dk} = \frac{\mathcal{R}}{\pi} + \frac{d\delta(k)}{dk}$ is approximately uniform in this case, because the phase shift does not depend on $\mathcal{R}$ and thus the last term in the density of states can be neglected compared to the first one.

So the Friedel oscillations are

$$n(r) - n_0 = \frac{1}{\pi^2}\int_0^{k_F}\sum_l (2l+1)k^2(R_{k,l}(r)^2 - j_l^2(kr))dk. \tag{3.1}$$

For the same reason as above, namely that the $R_{k,l}(r)$ are very similar to the $j_l(kr)$ for $l > kR_c$ one can carry out the l-sum in the integral just up to kR_c.

3.6. Summary of the Equations used in the Computer Program

3.6.1. *The Case* $\mathcal{R} = R_c$

The following equations are used for each iteration step of the self consistency loop:

1. The initial potential is $V_{eff}^{i,initial}(r)$, which comes from the previous iteration step for $i > 1$ or can be calculated from the starting density for $i = 1$.

2. With the definition $u_{E,l}(r) = rR_{E,l}(r)$, the usage of atomic units, and our approximations in this chapter the Schroedinger equation (2.17) turns into:

$$u_{E,l}''(r) = (2V_{eff}^{i,initial}(r) + \frac{l(l+1)}{r^2} - E)u_{E,l}(r).$$

This equation is solved numerically for the bound and scattered states. [1]

The boundary conditions for both the bound and the scattered states are: $u_{E,l}(r) = r^{(l+1)}$, $u_{E,l}(r) = (l+1)r^l$ at the inner cut-off radius and $u_{E,l}(r) = 0$ at the outer cut-off radius. The bound and scattered states give discrete energy eigenvalues, are automatically orthogonal (because the Hamiltonian is Hermitian for all wave-functions with the required boundary conditions), and can be normalized to unity.

3. Calculating the new density gives $n(r) = \frac{1}{4\pi} \sum_{n,l}^{all} deg(l) \frac{u_{n,l}^2(r)}{r^2}$, for spherically averaged systems. $deg(l)$ is equal to $2(2l+1)$ (the factor 2 is because spin degeneracy and the factor $2l+1$ because of m-degeneracy) except for the energetically highest state, in which case it is the total number of electrons in the system minus the number of already populated states. This choice forces the number of occupied states to be equal to the number of electrons in the system.

4. Then one calculates the output single particle kinetic energy

$$T = \sum_{n,l}^{all} deg(l) E_{n,l} + 2 \cdot 4\pi \int_{r_c}^{R_c} r^2 n(r) \mathcal{V}_{eff}^{i,initial}(r) dr,$$

and the Coulomb energy from (2.23) using

$$\int \frac{n(r') - n_0}{|\vec{r} - \vec{r}'|} d^3\vec{r}' =$$

---

[1] In order to use the SLATEC library-routines to solve differential equations the Schroedinger equation had to be converted to the equivivalent first-order system

$$\begin{pmatrix} u_{E,l}(r) \\ u'_{E,l}(r) \end{pmatrix}' = \begin{pmatrix} 0 & 1 \\ 0 & 2\mathcal{V}_{eff}^{i,initial}(r) + \frac{l(l+1)}{r^2} - E \end{pmatrix} \begin{pmatrix} u_{E,l}(r) \\ u'_{E,l}(r) \end{pmatrix}.$$

$$\int_0^\pi \int_0^{2\pi} \int_{r_c}^{R_c} (n(r') - n_0)(\sum_l \frac{r_<^l}{r_>^{l+1}} P_l(\cos\gamma))r'^2 \sin\gamma d\gamma d\phi dr' =$$

$$2\pi \int_{r_c}^{R_c} [\sum_l r'^2(n(r') - n_0)\frac{r_<^l}{r_>^{l+1}} \int_{-1}^1 P_l(x)dx]dr',$$

where $r_> = max(r, r')$, $r_< = min(r, r')$ and $P_l(x)$ are the Legendre polynomials. With $P_0(x) = 1$ and $\int_{-1}^1 P_l(x)P_0(x)dx = 2 \cdot \delta_{l,0}$ this simplifies to

$$4\pi[\frac{1}{r} \int_{r_c}^r r'^2(n(r') - n_0)dr' + \int_r^{R_c} r'(n(r') - n_0)dr'].$$

So

$$C = 4\pi \int_{r_c}^{R_c} r(n(r) - n_0)[4\pi \int_{r_c}^r r'^2(n(r') - n_0)dr') +$$

$$4\pi r \int_r^{R_c} r'(n(r') - n_0)dr' - 2 \cdot Z]dr.$$

Also the exchange correlation energy (2.27) can be obtained from the density, which simplifies for the spherical case to $E_{xc}[n] = 4\pi \int_{r_c}^{R_c} r^2 e_{xc}(n(r))n(r)dr$. Adding these three contributions gives the output energy.

5. The final effective potential can be simplified by using the same expansion for $\frac{1}{|\vec{r} - \vec{r'}|}$ as before. This gives

$$eV_{eff}^{i,final}(r) = 4\pi[\frac{1}{r} \int_{r_c}^r r'^2(n(r') - n_0)dr' + \int_r^{R_c} r'(n(r') - n_0)dr'] - \frac{2Z}{r} + \mu_{xc}(n(r)),$$

where μ_{xc} is the exchange correlation potential. Then this potential is normalized so that $V_{eff}^{i,final}(R_c) = 0$, in order to get a continuous transition to the zero potential for $r > R_c$.

6. The last step is to apply the mixing described in 3.1 to calculate the initial potential for the next iteration steps $V_{eff}^{i+1,initial}(r)$.

After a few iteration steps the calculated output energy should not change anymore. The obtained value is the energy of the system. Since the k-spectrum for the scattered states is discrete, the concept of phase shifts cannot be applied to calculate the immersion energy directly. Hence to get the immersion energy one has to run the program twice, a second time with the same background density but with $Z = 0$. This gives the energy of the pure system. The difference is the immersion energy.

3.6.2. *The Case $\mathcal{R} \to \infty$*

The steps 1, 5, 6 are the same as in the previous case. In step 2 the Schroedinger equation and the boundary conditions at the inner cut-off radius are the same. At the outer cut-off radius the boundary condition for the bound states are $u_{E,l}(R_c) = e^{(-\sqrt{-E}R_c)}$ and $u'_{E,l}(R_c) = -\sqrt{-E}e^{(-\sqrt{-E}R_c)}$. The boundary conditions on the scattered states are $u_{E=k^2,l}(R_c) = R_c j_l(kR_c)\cos\delta_l(k) - R_c n_l(kR_c)\sin\delta_l(k)$, which is just a normalization statement. The energy spectrum for $E > 0$ is continuous. Hence one solves the equation on an entire k-mesh $k = 0\ldots k_F$. The phase shift defined in section 2.5 are for the spin-independent, spherical case given by [2]

$$\tan\delta_l(k) = \frac{kR_c j'_l(kR_c)u_{k,l}(R_c) + j_l(kR_c)u_{k,l}(R_c) - R_c j_l(kR_c)u'_{k,l}(R_c)}{kR_c n'_l(kR_c)u_{k,l}(R_c) + n_l(kR_c)u_{k,l}(R_c) - R_c n_l(kR_c)u'_{k,l}(R_c)} \quad (3.2)$$

The phase shifts are determined up to an integer times π. Since the n_l and n'_l are not finite if their argument goes to zero but the j_l and j'_l are, $\tan\delta_l(k)$ goes to zero if k goes to zero. Hence we define $\delta_l(0) = 0$. Since we also need derivatives of phase

---

[2]To be precise the phase shifts are given by the limit$_{R_c \to \infty}$ of the left hand side of the equation. If R_c is large enough the limit-process can be ignored. The convergence of the phase shifts with R_c was automatically checked by the program by calculating the phase shifts for a series of R_c and checking if the values were independent on R_c.

shifts with respect to k, we have to define the phase shifts continuous in k. In this way the definition $\delta_l(0) = 0$ determines all phase shifts with no ambiguity in adding multiples of π.

One can also see that the phase shifts are independent of the normalization of $u_{k,l}$, so one can indeed define the normalization of u after calculating the phase shifts.

A brief discussion of the numerical error in calculating phase shifts is given in Appendix D.

From the fact that the scattered states do not approach zero fast enough for large r it follows that the Hamiltonian is not really Hermitian for these states. The scattered states and bound states are not automatically orthogonal anymore. This can lead to the phenomenon of ghost states, i.e. a shallow bound state can also contribute to the conduction electron density. This leads to an over-counting of electrons. In our calculation this effect was observed, when a bound state was just about to vanish for following iteration steps. So one has to check the results to make sure that the charge balance of the system is right, by integrating charge densities and comparing to the Friedel sum. This is explained in more detail in the next chapter.

Step 3 is for this case

$$n(r) - n_0 = \frac{1}{4\pi} \sum_{n,l}^{bound} 2(2l+1) \frac{u_{n,l}^2(r)}{r^2} + \frac{1}{\pi^2} \int_0^{k_F} \sum_l (2l+1)k^2 \left(\frac{u_{k,l}^2(r)}{r^2} - j_l^2(kr) \right) dk.$$

Note that now there is no restriction on the number of electrons in the sphere and hence all bound states are occupied.

In step 4 one can calculate the immersion energy directly for this case. So one has to run the program only once. Equation (2.26) is easily specialized to the present case:

$$E_{imm} = \sum_{n,l}^{bound} 2(2l+1)E_{n,l} + 2 \cdot 4\pi \int_{r_c}^{R_c} r^2 e \mathcal{V}_{eff}^{i,initial}(r)n(r)dr -$$

$$E_F \frac{1}{\pi} \sum_l 2(2l+1)\delta_l(E_F) - \frac{1}{\pi} \sum_l 2(2l+1) \int_0^{E_F} \delta_l(E)dE +$$

$$4\pi \int_{r_c}^{R_c} r(n(r)-n_0)[4\pi \int_{r_c}^{r} r'^2(n(r')-n_0)dr') +$$

$$4\pi r \int_r^{R_c} r'(n(r')-n_0)dr' - 2 \cdot Z]dr + 4\pi \int_{r_c}^{R_c} r^2 e_{xc}(n(r))n(r)dr. \qquad (3.3)$$

4. RESULTS AND CONCLUSIONS

4.1. Convergence of the Algorithm

Theoretically the convergence of the algorithm should be such that for subsequent iteration steps changes in the calculated immersion energy become smaller and smaller and that one can determine this quantity to any desired precision. All one has to do is to use a sufficient number of iterations. This is, however, not true for real calculations. Because numerical errors accumulate the algorithm has a certain limit of precision. Also it is likely to happen that the algorithm converges for the first few iteration steps and then starts to diverge. Hence to characterize the convergence one has to introduce a quantity that indicates how well the algorithm is converged. We use the difference in input and output potentials for this quantity. For each iteration step one calculates $d_i = 4\pi \int (\mathcal{V}_{eff}^{initial,i}(r) - \mathcal{V}_{eff}^{final,i}(r))^2 r^2 dr$ and the immersion energy E_{imm}^i. Without numerical errors, $d_i \to 0$ and $E_{imm}^i \to E_{imm}$ for $i \to \infty$. This never happens for real calculations. The idea how to get rid of this lack of complete convergence is to plot E_{imm}^i versus d_i. As shown in fig. 4.1 a linear dependence can be assumed for small d_i. This also follows from theoretical considerations. Next one interpolates E_{imm}^i to $d = 0$ to get the result E_{imm}.

Fig. 4.2 shows how the densities converge. The densities are very large at the center, the location of the impurity atom. Then they decrease rapidly and show
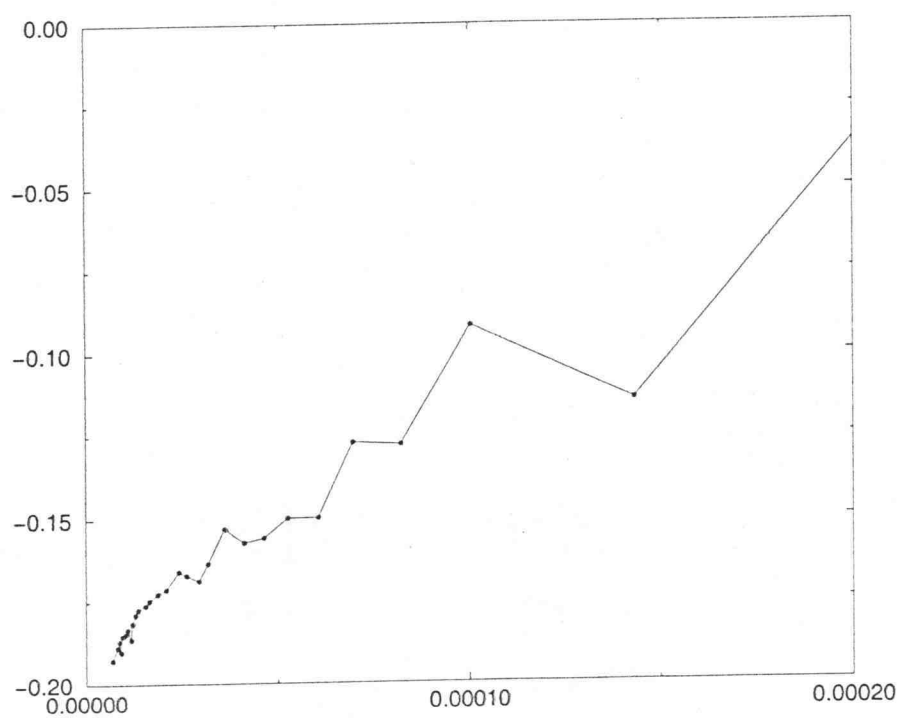
FIGURE 4.1. E_{imm}^i vs. d_i

Friedel oscillations. Analytical calculations predict (see [3, p. 235f]) that for large r, [1]

$$n(r) - n_0 \to \frac{1}{4\pi^2 r^3} \sum_l (2l + 1)(-1)^l sin(\delta_l(k_F)) \cdot cos(2k_F r + \delta_l(k_F)). \qquad (4.1)$$

To see the structure of the Friedel oscillations $r^3(n(r) - n_0)$ is plotted. The dense areas reflect the converged values for the density.

Fig. 4.3 shows a typical difference of an initial and a final potential. Since the potentials diverge like $\frac{1}{r}$ at the origin, r times the potential is plotted. For complete convergence the two potentials should be the same. This could, however, never be achieved in our calculations. The final potential is the one with the larger oscillations. This reflects the strong response of the system, which is the reason for divergence if no feedback of the potential is applied.

4.2. Precision of the Output Data

When preparing to run the program one is faced with making a choice for a large number of input parameters. There are the physical input parameters, the charge of the impurity atom Z and the background density n_0. Then there are the input parameters that determine the precision of the numerical calculations, namely the mesh in real space, the mesh in k-space for the scattered states, the tolerance energy for the bound states (E_{tol}), and the tolerance of the states for the differential equation solvers for both bound (ϵ_b) and scattered states (ϵ_s).

---

[1] Using this form for large r, it can be shown that the integral $4\pi \int_a^b r^2(n(r) - n_0)dr$ converges if $a \to \infty$ (in contrast to $\frac{1}{r} \cdot \frac{1}{r}cos(ar + b)$ can be integrated to infinity). Hence it is also possible to introduce an outer cut-off radius R, for the Friedel oscillations.
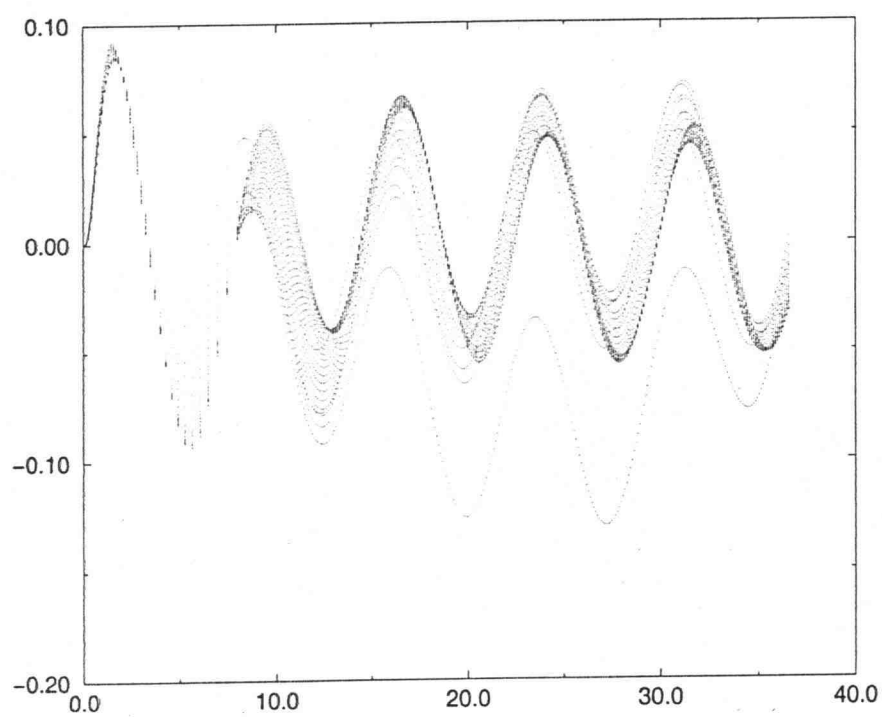
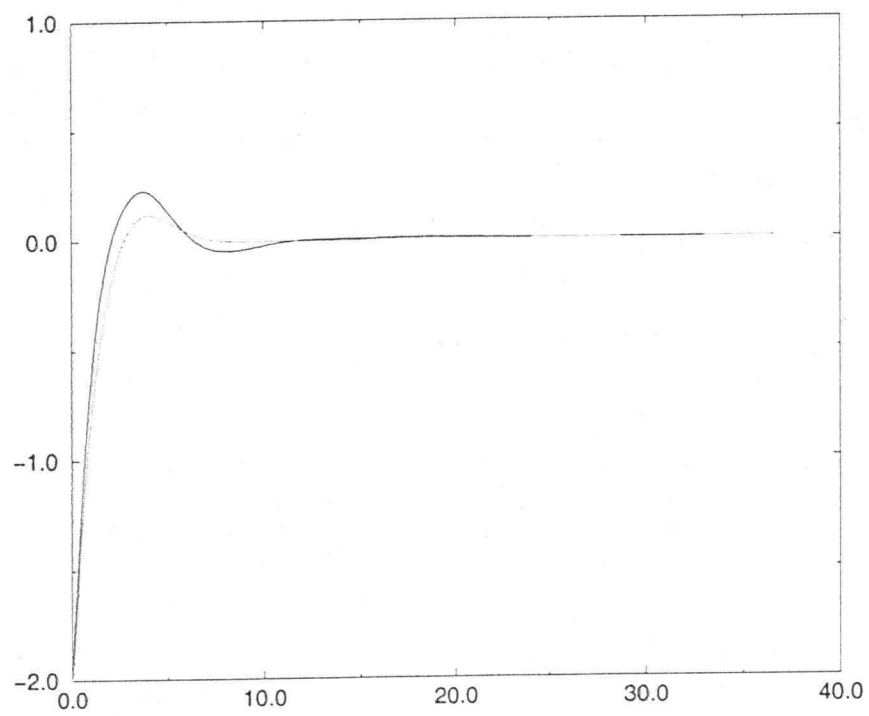FIGURE 4.2. $r^3(n(r) - n_0)$ vs. r for various iteration steps

FIGURE 4.3. $r\mathcal{V}_{eff}^{initial}$ and $r\mathcal{V}_{eff}^{final}$ vs. r

To account for the rapid change in potential close to the origin a logarithmic scale in real space was chosen from the inner cut-off radius r_c to a certain radius r_l, where the logarithmic scale was changed to a linear scale. The linear scale was from r_l to the outer cut-off radius R_c. In k-space a uniform mesh was chosen from 0 to the Fermi-wave-vector k_F with a step-size of k_{tol}.

Of course, the final results should only depend on the physical parameters, not on the numerical parameters.

One way to check the reliability of the output data is to run the second program for $Z = 0$. For this case the system is pure and the immersion energy is zero. If the output of the program is a value different from zero, this value is a lower boundary for the precision of the program. The resulting value was typically about 10^{-3}Ry. Another way to check the reliability of the output data is to produce independent data for which the results are already known. For the case with the $\mathcal{R} \to \infty$ boundary condition this can be a charge balance. Charge neutrality requires that an impurity atom with Z protons has to have Z electrons around it. One can now integrate $n(\vec{r}) - n_0$ over the sphere with radius R_c; this gives the extra number of extra electrons around the impurity atom and should be equal to Z. If these quantities do not agree, R_c was probably to small. In our calculations the error was typically around 1%. If Z_b is the number of bound states one can compare $Z - Z_b$ to the Friedel sum $\frac{2}{\pi} \sum_l (2l + 1)\delta_l(k_F)$. Both give the number of electrons in the conduction band and should be the same. The precision for this result was better than 1% in our calculations. When R_c was too small the agreement was not good, because the charge integration did not include all important Friedel oscillations and the phase shifts calculated at R_c were not converged yet. If R_c was too large the numerical error of the differential equation solver was too large when integrating outwards to R_c. Hence sometimes a suitable R_c has to be found by trial and error.

It turned out that in general 8 times the Wigner-Seitz radius is a good value for H. For Fe this value has to be lower.

The charge balance is automatically satisfied for the $\mathcal{R} = R_c$ boundary conditions. Hence charge balance cannot be used as a numerical check. For this case the Fermi-level can be calculated by the program and be compared to $E_F = 9\pi^{\frac{4}{3}} \cdot (n_0)^{\frac{2}{3}}$. Both should be the same. The agreement achieved was, however, not better than 10%.

A way to check the dependence of the results on the numerical parameters is to run the program for a series of different values of the same input parameter. The input parameters we used are such that the smaller value of the parameter corresponds to a better precision. Hence one can interpolate the results to zero to get the best precision for this input parameter. From this one can guess a good value for the parameter and the relative error for this value. This is done in Appendix C. It was found, however, that the precision depends also on the physical input parameters. For example, the larger n_0 is the smaller has to be ϵ_s; or the greater Z is the smaller has to be ϵ_s.

Typical input parameters are:

An r-mesh with $r_c = 10^{-5}$, $r_l = 2$, $R_c = 8r_{WS}$, 200 points on logarithmic scale and 300 points on linear scale. A k-mesh with about 60 k-points. $E_{tol} = 10^{-6}$, $\epsilon_b = \epsilon_s = 10^{-4}$ and about $20 - 30$ iteration steps.

4.3. Comparison of the two Cases of Boundary Conditions

The differences in immersion energies for the two cases are sometimes large. The reason is the large numerical error for the first case. Since two large energies are subtracted to calculate the small immersion energy, the relative error of the final results is immense. A way to reduce this error is to make R_c smaller for the

first program. Then the volume is smaller and so is the number of electrons in the system. This gives smaller total energies and thus smaller errors in the immersion energy. But if R_c is too small other numerical errors (see above) arise. Our general conclusion is that the second case is numerically much more appropriate and is preferred.

Fig. 4.4 is a plot of three output densities. The first one is the density calculated by the second program. The second one is the density calculated by the first program for the same physical input parameters, and the third density is also calculated by the first program but for the pure system. To see the features, r times the density is plotted and the first and third densities are displaced by 0.01 to the top and bottom, respectively. One can see that close to the origin, the first and second density agree, whereas close to the boundary the second and third density agree. This is very intuitive, since the effect of the boundary condition is strongest at the boundaries and gets weaker and weaker farther inside. The difference between the last two densities is very similar to the first density.

We conclude that the effect of boundary conditions for the first case is to produce density oscillations close to R_c that are much stronger than the Friedel oscillations and independent of the impurity atom. The difference in output densities for the two cases come from the boundary conditions. If R_c is large enough and boundary conditions can be neglected, both programs should produce the same output densities.
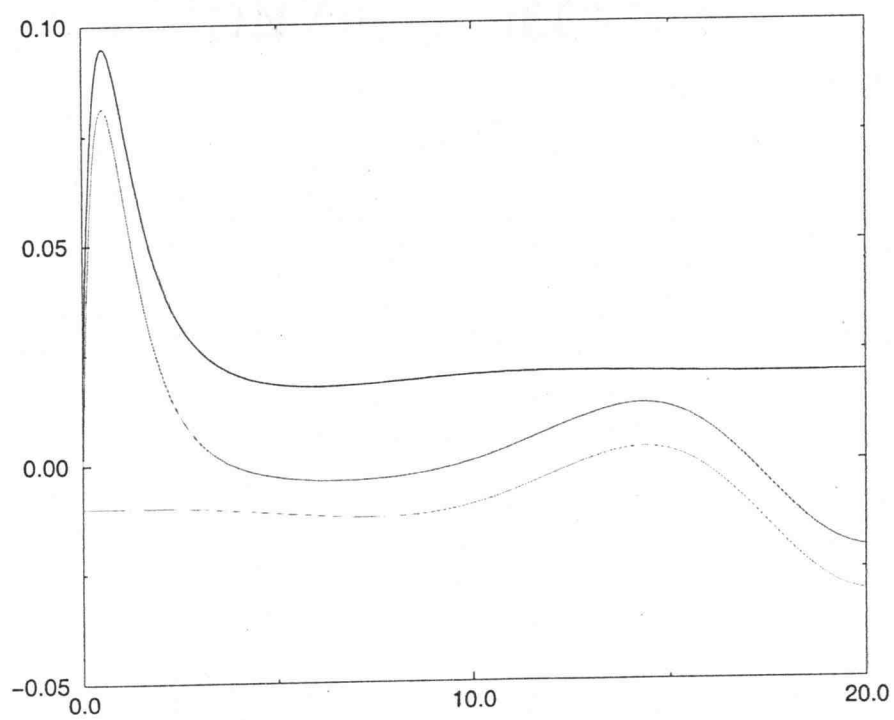
FIGURE 4.4. r times densities vs. r

4.4. Results for H

Results for H ($Z = 1$) were calculated for 14 different background densities. In Fig. 4.5 we give a plot of the electron densities for all 14 cases. From (4.1) it can be inferred that r^3 times the Friedel oscillations have a periodicity of $\frac{\pi}{k_F}$ in real space for large r. Hence we plotted the densities versus $k_F r$. Then the Friedel oscillations should have a periodicity of π, independent of the background charge. This is in very good agreement with our results.

The curves with the higher slopes at the origin and the larger oscillations correspond to lower background densities. For larger $k_F r$ the electron configuration is independent of the background density.

Fig. 4.6 shows a plot of the effective single particle potentials $r \mathcal{V}_{eff}^{final}(r)$ for the 14 different background densities.

In Fig. 4.7 a typical phase shift behavior is given. The absolute values of the phase shifts increase with k for all l-channels. The higher the l-value, the faster is the convergence of the phase shifts to zero for $k \to 0$.

Figs. 4.8 and 4.9 show a plot of $Z_l = \frac{2}{\pi}(2l + 1)\delta_l(k_F)$ versus l. Z_l can be interpreted as the number of states induced in the l-channel. For higher values of n_0, Z_0 becomes lower and seems to converge to about -1.3. The opposite effect exists in the $l = 1$-channel. Here Z_1 increases with n_0 and seems to converge to about 0.2. Overall the values of Z_l oscillate with l for all densities. For $l \to \infty$ they converge to 0. This convergence is slower for higher background densities. This means that for larger n_0 more and more l-channels are required to describe the system completely. If l_{max} is the cut-off for the l-values, then $Z_{l_{max}} \approx 0$ has to hold in order to describe
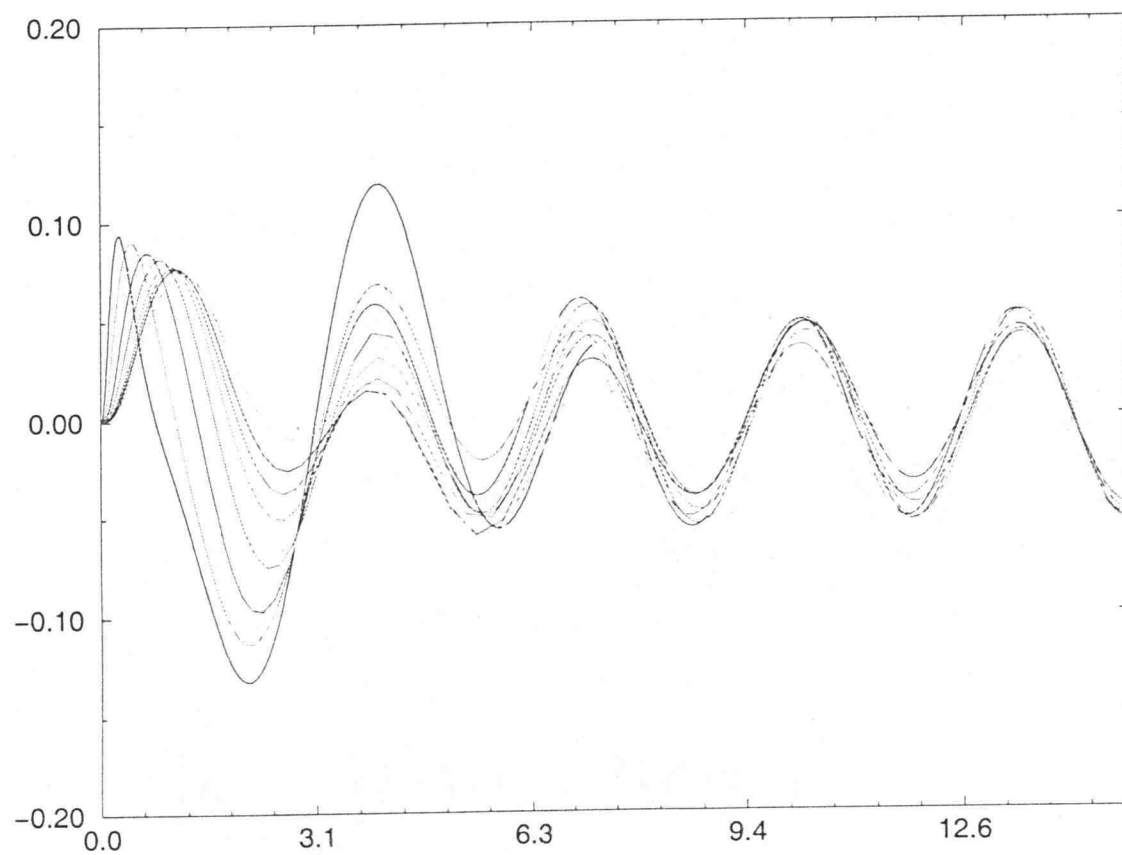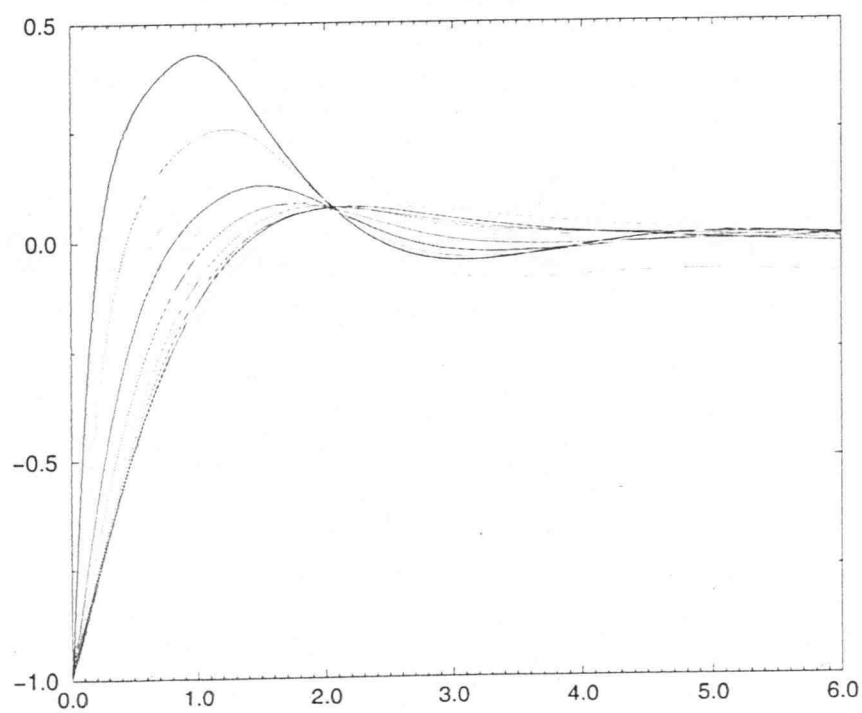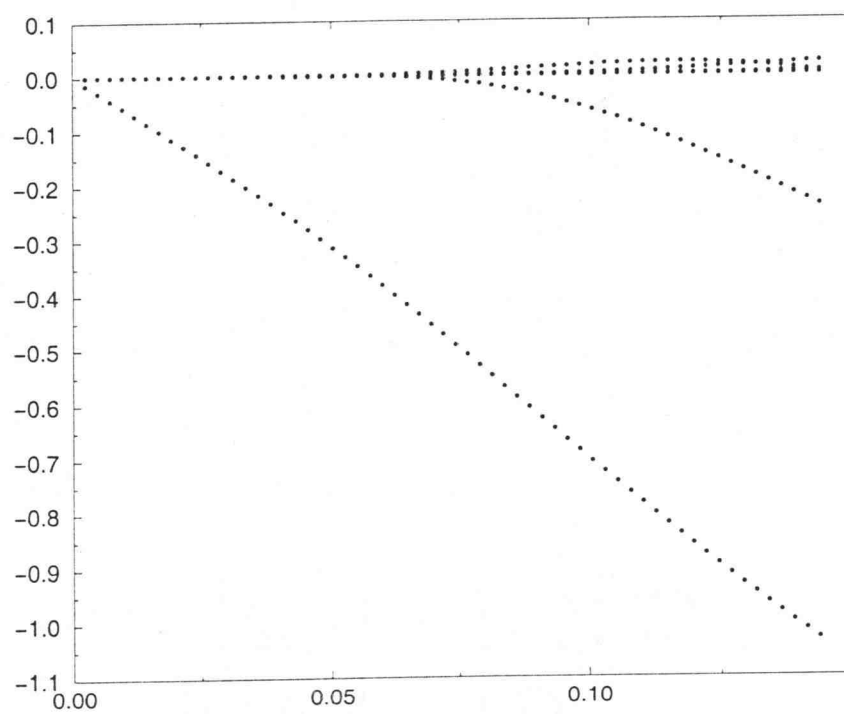
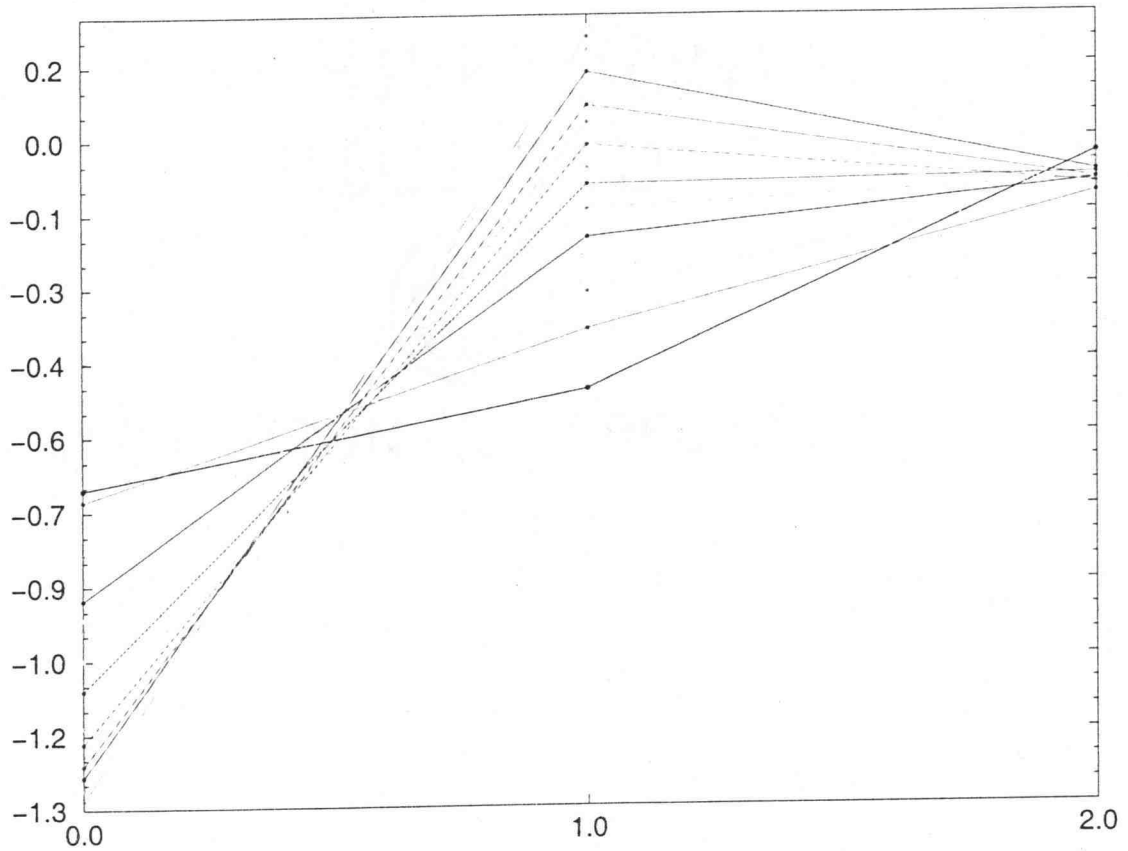FIGURE 4.5. r^3 times densities vs. $k_F r$

FIGURE 4.6. r times effective potentials vs. $k_F r$

FIGURE 4.7. $\delta_l(k)$ vs. k

FIGURE 4.8. Z_l vs. l

the system completely. This was always satisfied in our calculations; see the discussion in section 3.5.

Finally, Fig. 4.10 is a plot of the immersion energy versus background density. One sees a large negative slope at the origin, which corresponds to a stable H^- atom. The system has an equilibrium density $n_0 \approx 0.0025$ for H, where the immersion
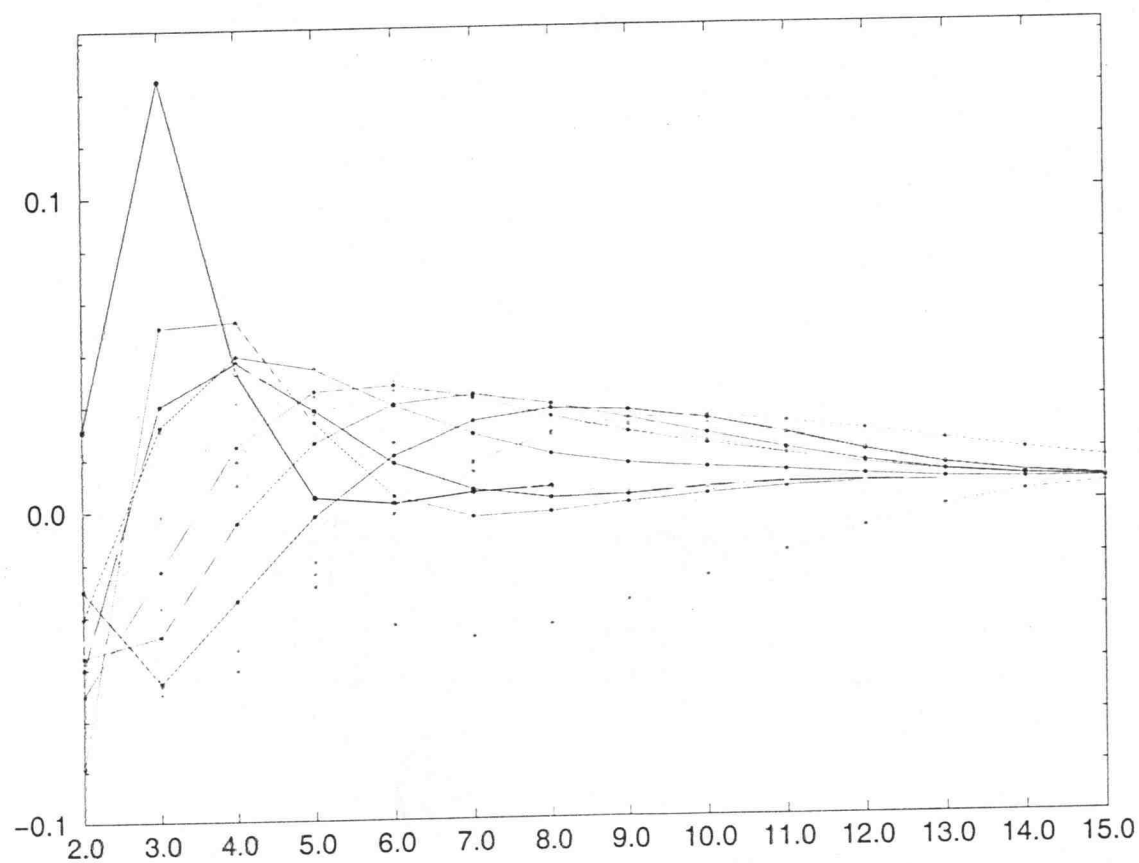
FIGURE 4.9. Z_l vs. l

energy is at minimum. At $n_0 \approx 0.022$ the immersion energy turns positive. For higher densities the immersion energy increases linearly with the background density.

Previously reported data points are taken from [10, FIG. 1.] and converted to atomic units:

$$n_0 = 0.0026 \quad E_{imm} = -0.13$$

$$n_0 = 0.005 \quad E_{imm} = -0.12$$

$$n_0 = 0.01 \quad E_{imm} = -0.07$$

$$n_0 = 0.015 \quad E_{imm} = -0.04$$

$$n_0 = 0.02 \quad E_{imm} = 0.0$$

$$n_0 = 0.025 \quad E_{imm} = 0.05.$$

$$n_0 = 0.03 \quad E_{imm} = 0.09.$$

It seems that our results are a little lower by a constant of 0.04Ry.

4.5. Results for Fe

For Fe ($Z = 26$) it was much harder to obtain converged results. The mixing ratio has to be as small as 0.001. Still the convergence was not good. The cut-off radius has to be reduced to about $R_c = 15$ in order to produce reasonable results for the phase shifts, which makes it hard to run the program for low densities since the range of the Friedel oscillations is too large in those cases. For higher densities the convergence properties are better. In the following table ranges for immersion energies are given:
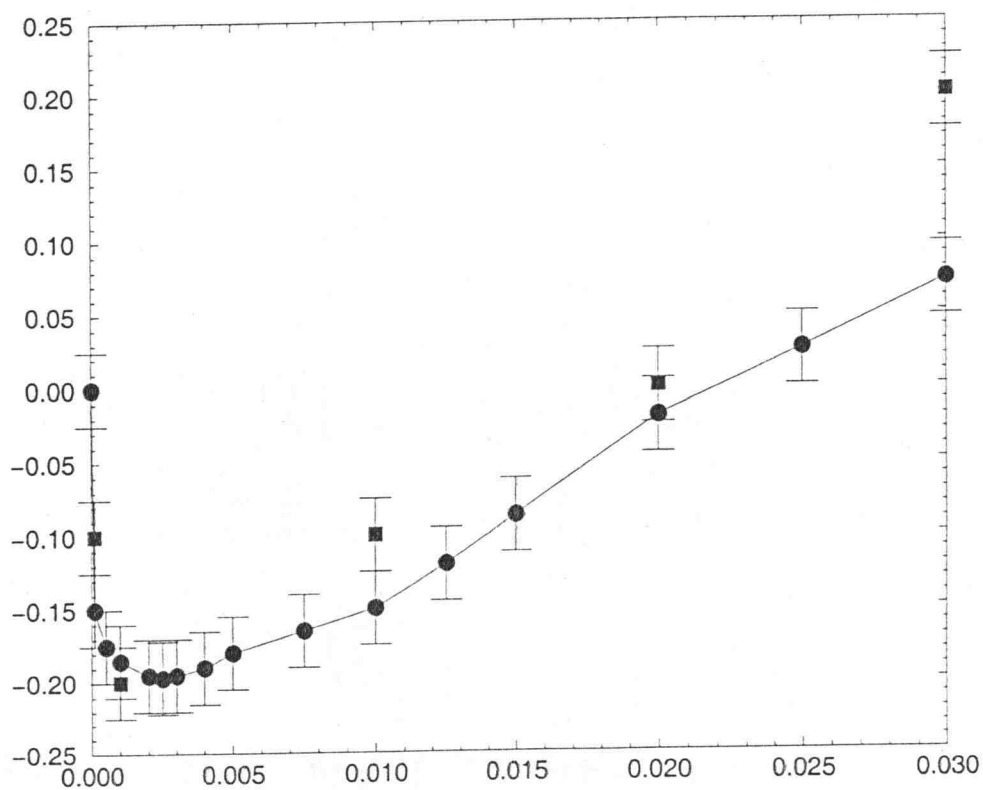
FIGURE 4.10. E_{imm} vs. n_0. Squares are the energies calculated with the first program, circles are the ones calculated with the second program.

$$n_0 = 0.001 \; E_{imm} = -2\ldots0$$

$$n_0 = 0.005 \; E_{imm} = -1\ldots1$$

$$n_0 = 0.01 \quad E_{imm} = 0\ldots0.5$$

$$n_0 = 0.02 \quad E_{imm} = -2.8\ldots-1.2$$

$$n_0 = 0.03 \quad E_{imm} = -1\ldots0$$

$$n_0 = 0.1 \quad E_{imm} = 8.3.$$

It seams that in the density range below 0.03 the immersion energy is about zero. This suggests that the interesting density range for Fe might be higher as for H. This has to be checked in the future.

In fig. 4.11 the output densities are plotted for different background densities and fig. 4.12 is a plot of the bound states for $n_0 = 0.03$.

4.6. Conclusions

Convergence could be achieved for hydrogen as an impurity atom for a variety of background densities. After suitable input parameters are found the results compare well to the already known results.

The convergence for iron has to be improved. This could just be a question of finding the right input parameters, but perhaps the program has to modified in order to have better convergence properties for large Z and strong effective potentials. These could be modifications in the feedback function. One idea is to make the mixing dependent on d_i, so one can systematically search for potential that lowers d_i. One can also try to mix densities instead of potentials.

In addition we need to investigate the role of partial occupation of the d-shell.
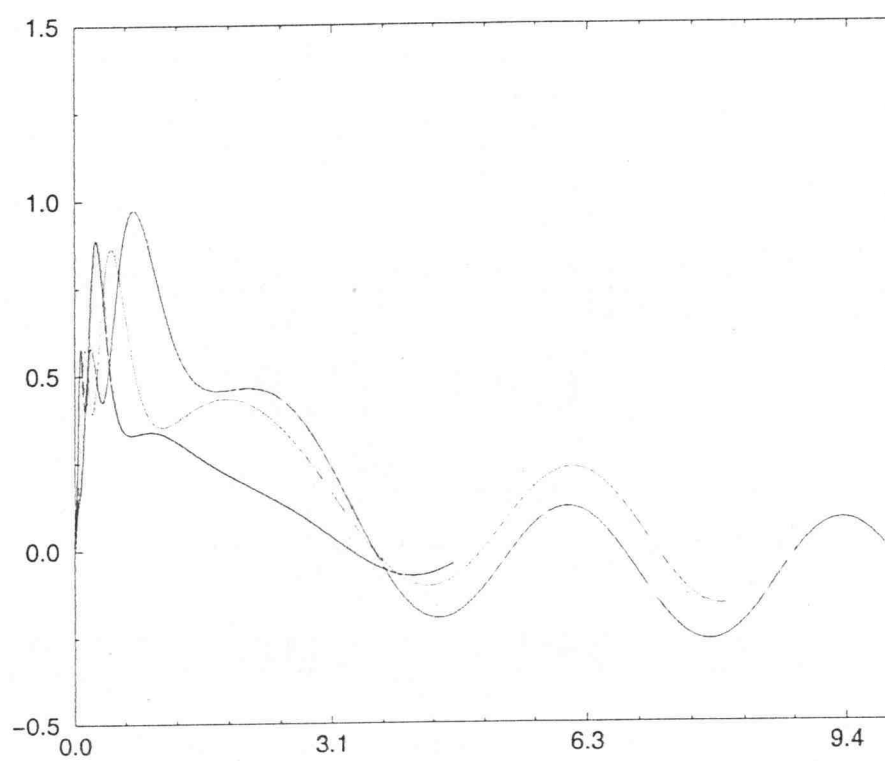
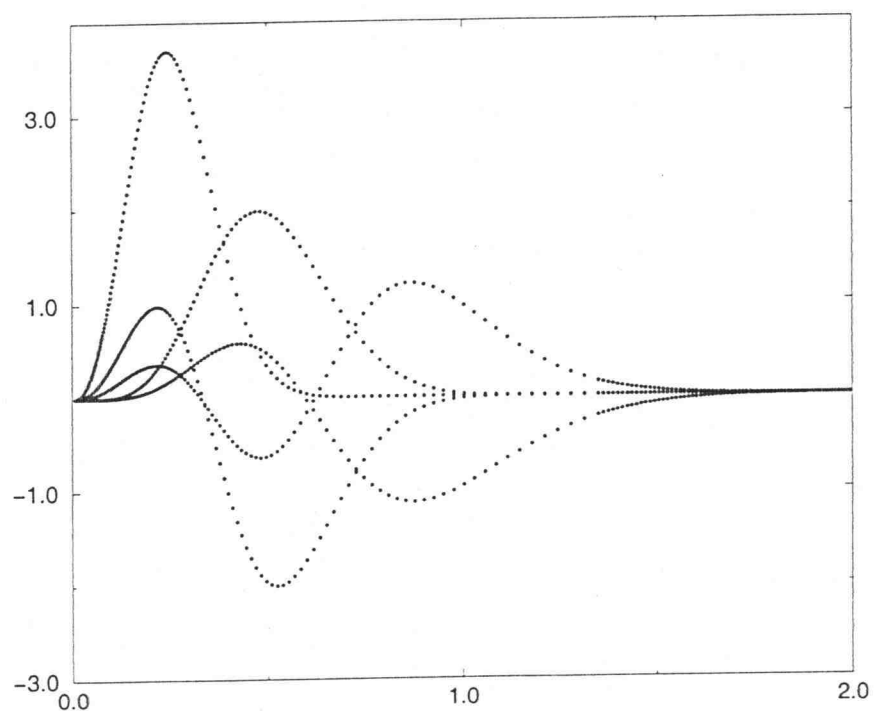FIGURE 4.11. r^3 times densities for Fe vs. $k_F r$

FIGURE 4.12. $u_{n,l}(r)$ for $n_0 = 0.03$

BIBLIOGRAPHY

[1] S. Lundquist, N.H. March, *Theory of the inhomogeneous electron gas*, [Plenum Press, 1983]

[2] R.M. Dreizler, E.K.U. Gross, *Density Functional Theory*, [Springer-Verlag, 1990]

[3] G.D. Mahan, *Many-Particle Physics*, [Plenum Press, 1981]

[4] R.G. Newton, *Scattering theory of waves and particles*, [Springer-Verlag New York, Inc.]

[5] C. Cohen-Tannoudji, *Quantum mechanics* [Wiley-Interscience]

[6] J.D. Jackson *Classical Electrodynamics*, [John Wiley & Sons, Inc.]

[7] R.H. Landau, M.J. Paes, *Computational Physics*, [John Wiley & Sons, Inc.]

[8] M. Abramowitz, I.A. Stegun, (editors) *Handbook of Mathematical Functions* [Dover Publications, Inc.]

[9] F.G. Fumi, "Vacancies in Monovalent Metals", *Phil. Mag.* vol. 46 (1955), pp. 1007ff

[10] M.J. Puska, R.M. Nieminen, M. Maninen, "Atoms embedded in an electron gas: Immersion energies", *Physical Review B* vol. 24,# 6 (1981), pp. 3037ff

[11] O. Gunnarsson, B.I. Lundquist, "Exchange and correlation in atoms, molecules, and solids by the spin-density-functional formalism", *Physical Review B* vol. 13,# 10 (1976), pp. 4274ff

[12] U. von Barth, L. Hedin, "A local exchange-correlation potential for the spin polarized case: I" *Journal of Physics* vol. 5 (1972), pp. 1629ff

APPENDICES

APPENDIX A. Spin-Dependent Hamiltonian

The full spin-dependent, non-relativistic Hamiltionian is:

$$\widehat{H} = \sum_{s,s'} \int \Psi_s^\dagger(\vec{r})[-\frac{\hbar^2}{2m}\vec{\nabla}^2\delta_{s,s'} + V^{s,s'}(\vec{r})]\Psi_s(\vec{r})d^3\vec{r} +$$

$$\frac{1}{2}\sum_{s,s'}\int\int\Psi_s^\dagger(\vec{r})\Psi_{s'}^\dagger(\vec{r'})\frac{q^2}{|\vec{r}-\vec{r'}|}\Psi_{s'}(\vec{r'})\Psi_s(\vec{r})d^3\vec{r}d^3\vec{r'}. \tag{A1}$$

For spin $\frac{1}{2}$ particles we have $V^{s,s'}(\vec{r}) = V(\vec{r})\delta_{s,s'} - \frac{1}{2}\mu_0\vec{B}(\vec{r})\cdot\vec{\sigma}_{s,s'}$, where $V(\vec{r})$ is the spin-independent potential, $\vec{B}(\vec{r})$ is the magnetic field, and $\vec{\sigma}$ is the vector of Pauli-matrices. The density matrix is given by

$$n^{s,s'}(\vec{r}) = <\Phi|\Psi_s^\dagger(\vec{r})\Psi_{s'}(\vec{r})|\Phi>.$$

Since the density matrix is Hermitian and $L-S$-coupling is ignored it can be diagonalized. The total density is $n(\vec{r}) = Tr[n^{s,s'}(\vec{r})]$. With the assumption that $B_x = B_y = 0$ and

$$\sigma_z = \begin{pmatrix} 1 & 0 \\ 0 & -1 \end{pmatrix}$$

one gets for the matrix of the potential

$V^{+,-}(\vec{r}) = V^{-,+}(\vec{r}) = 0,$

$V^+(\vec{r}) := V^{+,+}(\vec{r}) = V(\vec{r}) + \mu_0 B_z(\vec{r})$ and

$V^-(\vec{r}) := V^{-,-}(\vec{r}) = V(\vec{r}) - \mu_0 B_z(\vec{r}).$

This leads exactly to (2.1). All theorems in chapter 2 are valid for this simplified potential. They can, however, be extended to the general Hamiltonian if one works with the density matrix $n^{s,s'}(\vec{r})$.

The reader may ask why spin dependent potentials are considered at all in this thesis at all, because in the case of immersion energies, we have set $B_z(\vec{r}) = 0$. The reason is that most exchange energies are parameterized by the diagonal elements

of the density matrix. By introducing a spin-dependent potential one naturally incorporates these diagonal elements into the notation right from the beginning. Another reason is that one can describe spin-polarized systems with the formalism, which is, however, not done in this thesis.

APPENDIX B. Supplement on Proof of HK Theorem

In the following the only part of the proof in [2, sec. 2.1] for which generalization to spin dependent potentials is not obvious, is extended to these potentials. Equation (2.6) in the book states

$$(\widehat{V} - \widehat{V}')|\Phi> = (E_{gs} - E'_{gs})|\Phi>,\qquad\text{(B1)}$$

where the generalized potentials are now

$$\widehat{V} - \widehat{V}' = \sum_s \int \Psi_s^\dagger(\vec{r})[V^s(\vec{r}) - V'^s(\vec{r})]\Psi_s(\vec{r})d^3\vec{r}.\qquad\text{(B2)}$$

From this it can be concluded $\widehat{V} - \widehat{V}' = E_{gs} - E'_{gs}$.

This can be achieved in the following way: Multiplying eqn. (B1) from the left by

$$<\vec{x}_1,...,\vec{x}_N|^{s_1,...,s_N} = <0|\Psi_{s_1}(\vec{x}_N)...\Psi_{s_N}(\vec{x}_1)$$

(N is the number of particles, $<0|$ the vacuum state) gives with the definition

$$\psi^{s_1,...,s_N}(\vec{x}_1,...\vec{x}_N) = <0|\Psi_{s_1}(\vec{x}_N)...\Psi_{s_N}(\vec{x}_1)|\Phi>:$$

$$\sum_s \int [V^s(\vec{r}) - V'^s(\vec{r})]d^3\vec{r} <0|\Psi_{s_1}(\vec{x}_N)...\Psi_{s_N}(\vec{x}_1)\Psi_s^\dagger(\vec{r})\Psi_s(\vec{r})|\Phi> =$$
$$(E_{gs} - E'_{gs})\psi^{s_1,...,s_N}(\vec{x}_1,...\vec{x}_N)$$

This turns after using the anti-commutation relations

$$[\Psi_{s_i}(\vec{x}_i), \Psi_s(\vec{r})]_+ = 0 \text{ and } [\Psi_{s_i}(\vec{x}_i), \Psi_s^\dagger(\vec{r})]_+ = \delta_{s,s_i}\delta(\vec{x}_i - \vec{r})$$

$(1 \leq i \leq N)$ N times with $<0|\Psi_s^\dagger(\vec{r}) = 0$ into

$$\sum_i [V^{s_i}(\vec{x}_i) - V'^{s_i}(\vec{x}_i)]\psi^{s_1,\ldots,s_i,\ldots,s_N}(\vec{x}_1,\ldots,\vec{x}_i,\ldots,\vec{x}_N) =$$

$$(E_{gs} - E'_{gs})\psi^{s_1,\ldots,s_N}(\vec{x}_1,\ldots,\vec{x}_i,\ldots,\vec{x}_N).$$

From this follows for well-behaved potentials

$$V^s(\vec{r}) - V'^s(\vec{r}) = \frac{E_{gs} - E'_{gs}}{N}$$

and so with (B2)

$$\widehat{V} - \widehat{V}' = \frac{E_{gs} - E'_{gs}}{N} \sum_s \int \Psi_s^\dagger(\vec{r})\Psi_s(\vec{r}) d^3\vec{r} = E_{gs} - E'_{gs}.$$

APPENDIX C. Discussion of the Error Bars

In the following the figures (4.13 - 4.16) of the dependency of the immersion energy on the typical input parameters are given. Linear regression was used to extrapolate the curves to zero. The intersection of the regression at zero was used as a basis to estimate the relative errors.

Including all errors of these four parameters into the error of the immersion energy gives a total error of about $\sqrt{(5\%)^2 + (9\%)^2 + (1\%)^2 + (7\%)^2} = 12\%$. The error bars for the immersion energy in chapter 4 are based on this value.

APPENDIX D. Phase Shift Errors

Fig. 4.17 is a log-log plot of the phase-shifts of $l = 0$ and a zero potential versus k. The phase-shifts should be identical to 0. One can see that for $log(k) < 0$ this is satisfied to an accuracy of $10^{(-6)}$. But for $log(k) > 0$ the error of $log(\delta_0(k))$ increases linearly with $log(k)$ with a slope of 6. The same characteristic behavior
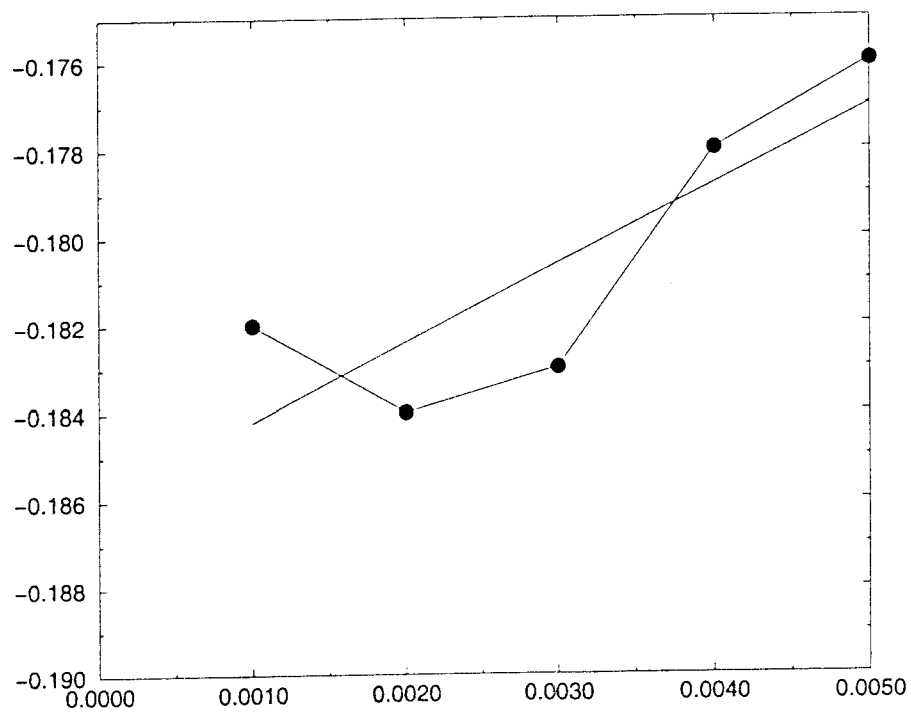
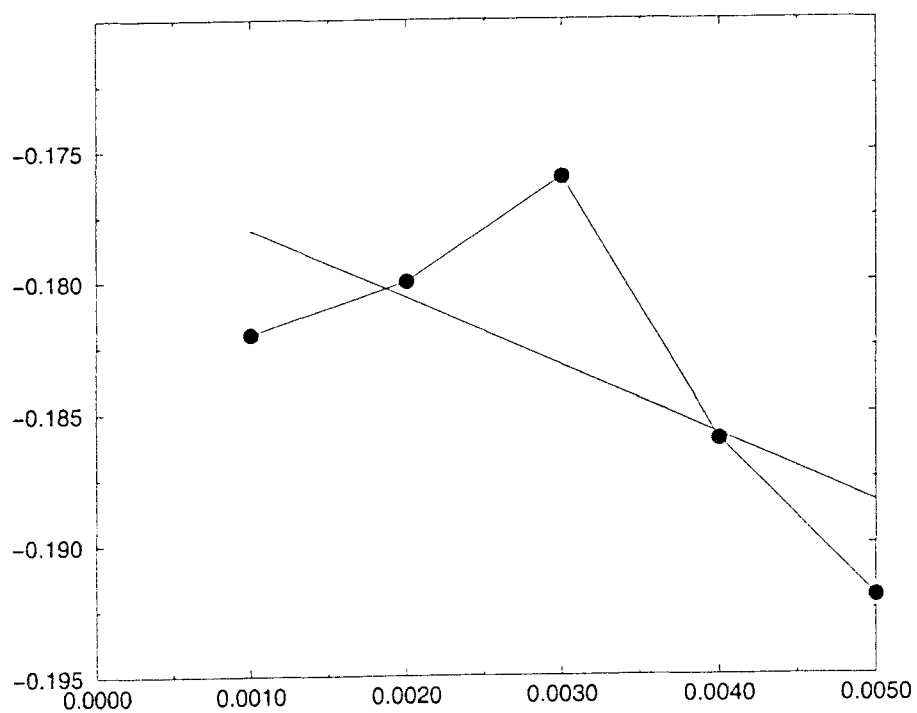FIGURE 4.13. E^i_{imm} vs. ϵ_b. The maximum relative error for the points in this plot is about 5%.

FIGURE 4.14. E^i_{imm} vs. ϵ_s. The maximum relative error for the points in this plot is about 9%.
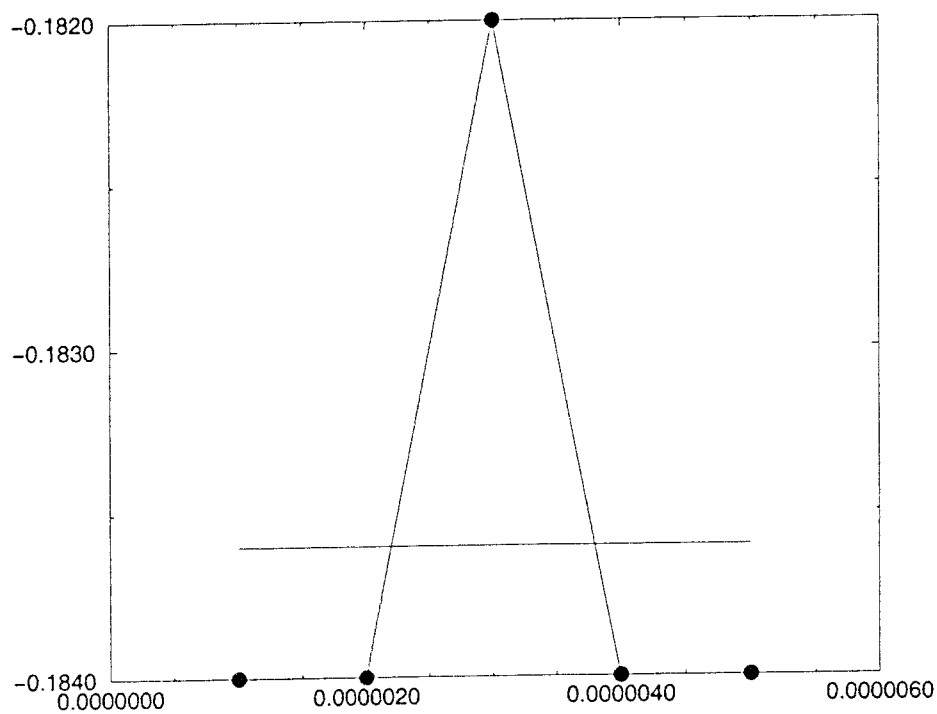
FIGURE 4.15. E^i_{imm} vs. E_{tol}. The maximum relative error for the points in this plot is about 1%.
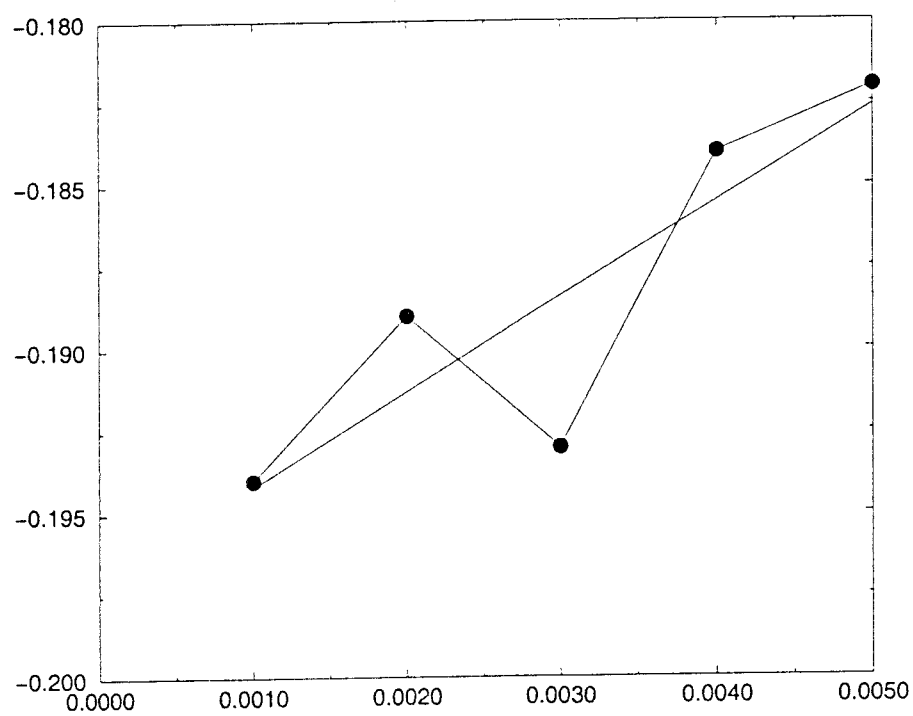
FIGURE 4.16. E^i_{imm} vs. k_{tot}. The maximum relative error for the points in this plot is about 7%.
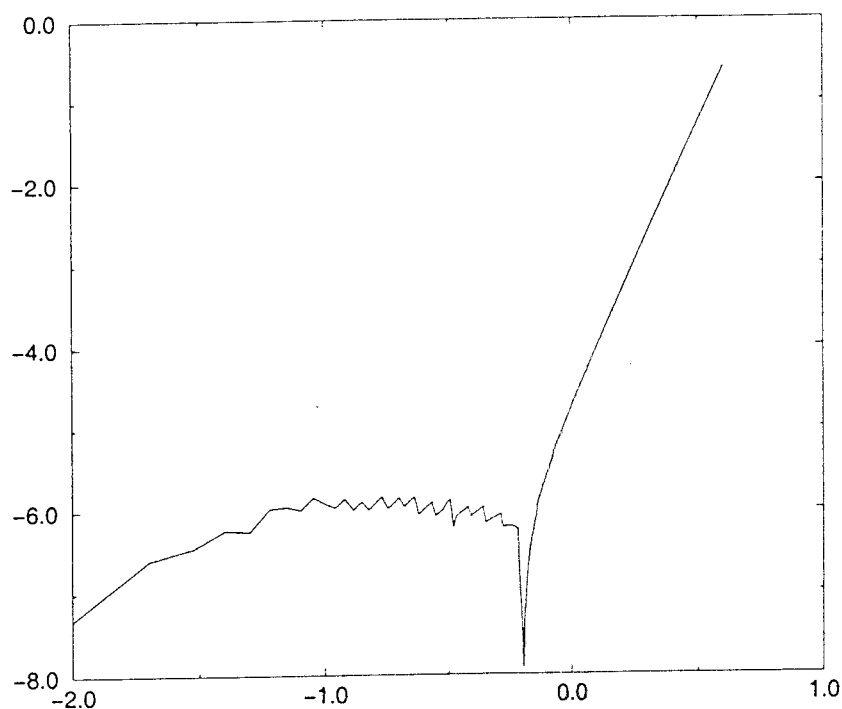
FIGURE 4.17. $log\delta_0(k)$ vs. $log(k)$

was found for higher l-terms. This means the error in phase-shifts goes with k^6. This is the reason for higher errors in the immersion energies if n_0 (and thus the Fermi-level) is higher. This error is due to the integration routines.

APPENDIX E. Special Functions used in this Thesis

A lot of this material can be found in [6].

The Legendre polynomials are

$$P_l(x) = \frac{1}{2^l} \sum_{m=0}^{[\frac{l}{2}]} (-1)^m \binom{l}{m} \binom{2l - 2m}{l} x^{l-2m},$$

where $\binom{a}{b} = \frac{a!}{b!(a-b)!}$ and $[\frac{l}{2}]$ is the largest integer smaller than or equal to $\frac{l}{2}$. The Legendre polynomials are orthogonal and $P(1) = 1$:

$$\int_{-1}^{1} P_l(x) P_{l'}(x) dx = \frac{2}{2l+1} \delta_{l,l'}.$$

The following expansion is valid:

$$\frac{1}{|\vec{r} - \vec{r'}|} = \sum_{l=0}^{\infty} \frac{r_<^l}{r_>^{l+1}} P_l(cos\gamma),$$

where $r_> = max(r, r')$, $r_< = min(r, r')$, and γ is the angle between $\vec{r}$ and $\vec{r'}$.

The spherical harmonics are

$$Y_{l,m} = \sqrt{\frac{2l+1}{4\pi} \frac{(l-m)!}{(l+m)!}} P_l^m(cos\theta) e^{im\phi}$$

for $-l \le m \le l$, where $P_l^m(x) = (-1)^m (1 - x^2)^{\frac{m}{2}} \frac{d^m}{dx^m} P_l(x)$. The $Y_{l,m}$ are a complete, orthonormal set of functions on the surface of a sphere. $Y_{l,m}$ is an eigen-function of the Casimir operators, $L^2 = -[\frac{1}{sin\theta} \frac{\partial}{\partial\theta}(sin\theta \frac{\partial}{\partial\theta}) + \frac{1}{sin^2\theta} \frac{\partial^2}{\partial\phi^2}]$ and $L_z = -i\frac{\partial}{\partial\phi}$, of the rotation group with eigen-values $l(l+1)$ and m, respectively.

The following expansion holds:

$$P_l(cos\gamma) = \frac{4\pi}{2l+1} \sum_{m=-l}^{l} Y_{l,m}^*(\theta', \phi') Y_{l,m}(\theta, \phi),$$

where $cos\gamma = cos\theta cos\theta' + sin\theta sin\theta' cos(\phi - \phi')$. Also we have the sum rule:

$$\sum_{m=-l}^{l} |Y_{l,m}(\theta, \phi)|^2 = \frac{2l+1}{4\pi}.$$

The spherical Bessel functions are defined by:

$$j_l(x) = \sqrt{\frac{\pi}{2x}} J_{l+\frac{1}{2}}(x)$$

and

$$n_l(x) = \sqrt{\frac{\pi}{2x}} N_{l+\frac{1}{2}}(x),$$

where $J_\nu(x)$ is the Bessel function of the first kind of order ν and N_ν is the Neumann function of order ν.

The functions $j_l(x)$ and $n_l(x)$ are linearly independent solutions of the differential equation:

$$[\frac{d^2}{dx^2} + \frac{2}{x}\frac{d}{dx} + 1 - \frac{l(l+1)}{x^2}]y(x) = 0.$$

$j_l(x)$ is finite at the origin and $n_l(x)$ diverges at $x = 0$.

The following limiting values are valid for large x:

$$j_l(x) \rightarrow \frac{1}{x} sin(x - \frac{l\pi}{2}),$$

$$n_l(x) \rightarrow -\frac{1}{x} cos(x - \frac{l\pi}{2}).$$